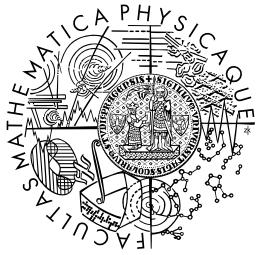

FACULTY
OF MATHEMATICS
AND PHYSICS
Charles University

MASTER THESIS

Michal Habera

Modeling of porous metal oxide layer growth in the anodization process

Mathematical Institute

Supervisor of the master thesis:	RNDr. Ing. Jaroslav Hron, Ph.D.
Study programme:	Physics
Study branch:	Mathematical and physical modeling in physics

Prague 2017

I declare that I carried out this master thesis independently, and only with the cited sources, literature and other professional sources.

I understand that my work relates to the rights and obligations under the Act No. 121/2000 Sb., the Copyright Act, as amended, in particular the fact that the Charles University has the right to conclude a license agreement on the use of this work as a school work pursuant to Section 60 subsection 1 of the Copyright Act.

In ..... date ..... signature of the author

Title: Modeling of porous metal oxide layer growth in the anodization process

Author: Michal Habera

Institute: Mathematical Institute

Supervisor: RNDr. Ing. Jaroslav Hron, Ph.D., Mathematical Institute

Abstract: Under suitable conditions anodic metal oxidation leads to growth of complex porous structures. The initiation and growth of these structures is an interesting and challenging task for electrochemical modelling. One must identify chemical reactions in a multi-phase framework, derive a proper partial differential equations and solve them in time dependent domains. In this work, electrochemical model for the oxide growth in nano scales is presented. Physically motivated equations are formulated with precise mathematical meaning and existence of solutions is studied. Electrostatic potential fulfilling high-field conduction law and interfacial jump conditions is sought for. Numerical discretization is performed with the use of finite element method and free boundaries are tracked with characteristic level-set functions. Basic mechanism governing the growth of porous structures is given and numerical experiments are explained on it's basis. This thesis presents novel contributions to the electrochemical and mathematical picture of nanopores growth.

Keywords: nanopores nanotubes elliptic interface level-set

To all who supported me.

To my family and my heartfriend Zuzana.

To my co-supervisor dr. Ondřej Souček, my supervisor dr. Jaroslav Hron, prof. Josef Málek and dr. Jan Macák. Without their guidance this thesis would not be thinkable.

"No man can ever lack this mortification of his vanity, that what he knows is but a very little in comparison of what he is ignorant of. Consider this, and instead of boasting thy knowledge of a few things, confess and be out of countenance for the many more which thou dost not understand."

Thomas a Kempis

Contents

Introduction

This master thesis is a compilation of results from different parts of physics, chemistry and mathematics.

It deals with a problem of metal oxidation, i.e. formation of oxides (TiO_2, Al_2O_3, $ZnO, MnO, \ldots$) on the surface of a corresponding metal. These oxides could form a nice compact surface coating with thicknesses in range $1 - 1000$ nm or it could develop into porous or tubular structures.

There are several physical and chemical models which capture such behaviour. Current picture of these processes is by no means complete. History of this topic and literature overview is given in first chapter. Applications of porous/tubular structures, especially on titan dioxide TiO_2 are discussed. We need to keep in mind that diversity of possible applications should be a driving force for this work.

In second chapter electrochemical model is examined in more detail. This part is formulated in language of **electrochemical engineering**.

Third chapter considers mathematical point of view on the electrochemical model. It is necessary to formulate equations in a precise way, study their properties (existence, uniqueness). This part is formulated in language of **mathematical analysis**.

Abstract mathematical formulation is a good starting point before **numerical discretization** is proposed. Keeping in mind what abstract mathematical properties belong to this problem one can implement finite element method to actually solve it. In the fourth chapter all details about discretization, implementation and convergence are given.

Fifth chapter shows results of numerical calculations. Convergence properties for a simple sub-problem are studied and general model is tested on several geometries.

How to read this thesis / how is it written

As we stated, this is a compilation of results from different parts of mathematical and physical sciences. In mathematics, it is recommended to communicate results in "definition-theorem-proof" style. In physical and chemical sciences more "continuous stories" are told. Although we fully understand the advantages [1] of mathematical approach, we choose physical way of presentation.

This text is written as a story. One task is followed by another and motivational link is given. On the other hand, we hope that mathematical exactness is not suppressed when it is needed.

[1] clarity of presentation, minimum unnecessary information

1. History and literature overview

1.1 History and literature

In this section we briefly review current state of research in nanopores modeling. Several terms (pore shape, dissolution rate, electric potential, ...) are not given precise meaning here. We do so in consequent chapters.

Historically, first results of some porous oxide structures were reported on aluminium. It dates back to [Keller et al., 1953]. Using optical and electron optical micrographs they observed regular, almost cylindrical, parallel-sided pores, perpendicular to the macroscopic surface. In additions, these pores formed close-packed hexagonal, cellular structure. It was postulated in their consequent works, that structure maintained itself during growth of oxide.

These observations triggered significant interest. The work on morphology and mechanism of formation of porous anodic films on aluminium due to [O'sullivan and Wood, 1970] is considered a classic reference.

We should stress here, that most of the pioneering work was done in the scope of **nanopores on alumina**. Difference between nanopores and nanotubes is rather subtle and many authors confuse the terminology. Think of nanopores as of porous holes etched into an oxide. In this thesis only nanopores are simulated.

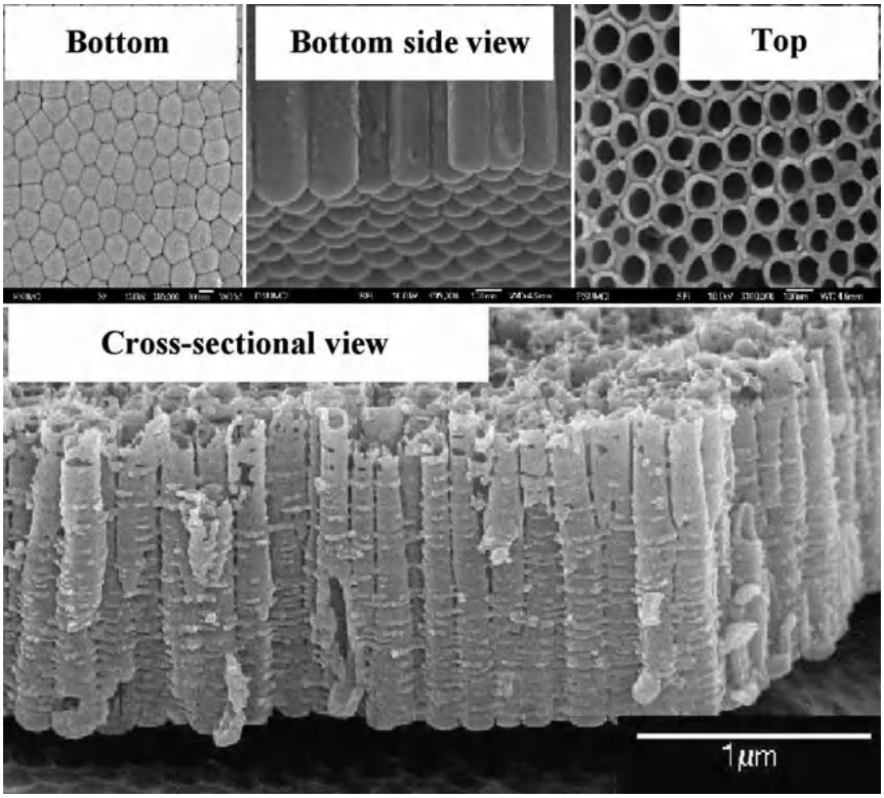

Figure 1.1: An example of experimentally grown nanotubes structure.
Taken from [Grimes and Mor, 2009].

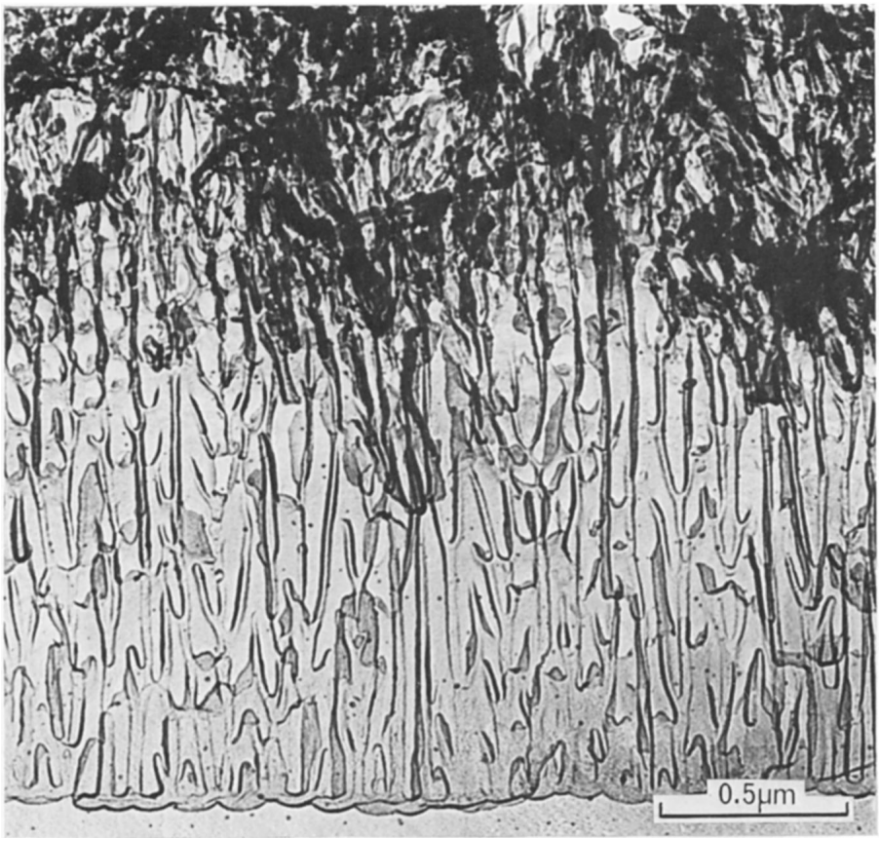

Figure 1.2: An example of experimentally grown nanopores structure.
Taken from [O'sullivan and Wood, 1970].

Another classical reference become [Parkhutik and Shershulsky, 1992]. With approx. 650 citations [1] their model of nanopores on alumina is considered essential, even in modern-days. They make quantitative predictions based on mechanism from [O'sullivan and Wood, 1970]. It is assumed, that pores are formed due to enhanced electric field at any surface perturbation. This field boosts electrochemical dissolution of oxide. On the other hand, new oxide is formed also with increased rate, so this counter-play determines final pore shape. They force the shape of pore to be stationary and hemispherical [2]. Aforementioned conditions give linear dependence of pore radius on applied electric potential – in agreement with experimental data. However, the exact form of dissolution rate vs. electric field is questionable.

We should mention here the model of [Cheng, 2015]. It is of Parkhutik & Shershulsky-type but geometry is not forced to be constant. They solve the equations over oxide phase and move it's boundaries accordingly. Discretized mesh must be re-meshed and additional smoothing is implemented to suppress its ragged shape. This smoothing could have crucial effect on pore stability. Furthermore, current continuity is imposed in a way, which requires reconstruction of electric current from potential. It involves path integration and most of computational time is consumed in this task.

[1] According to Google Scholar, April 2017.

[2] Note this condition carefully. In this thesis, similar model is used, but we do not force the shape of pore to some predefined geometry and this has substantial effects.

Next class of models are represented by [DeWitt and Thornton, 2014, 2016]. These models are very complex and solve spatio-temporal evolution of concentration of several ions. Ions migrate under high-field conduction mechanisms and reaction kinetics are prescribed. Nevertheless, the more complex model, the more "free" parameters emerge. Many parameters are given poor interpretation and cannot be experimentally measured.

We would like to focus on simpler models. Simple enough so all parameters have reasonable explanation but complex enough so all the desired phenomena (pore initiation, growth) are observable. Papers [Houser and Hebert, 2006, 2009, Hebert and Houser, 2009, Hebert et al., 2012] constitute this group. Many results in this thesis are built on [Houser and Hebert, 2006] electrochemistry. In their work, geometry is forced to be constant and velocity of oxide boundaries are computed from Laplace equation for potential and compared to velocity from current continuity equation. Velocity profile is not the same at both interfaces, which motivates them to incorporate plastic flow and stress generation into the model.

Papers [Limonov, 2011, Sample and Golovin, 2006] study instability of oxide surface. Their reaction kinetics are in addition curvature dependent, which is the crucial factor. Linear stability analysis of the equations leads to Kuramoto-Sivashinsky equation [3] with chaotic behaviour and short-wave stabilisation mechanism.

Let alone numerous experimentalists papers [Macak et al., 2007], where influence of electrolyte composition (pH, ion concentration, water content), temperature, age of electrolyte, potential sweeping rate, etc. are thoroughly studied.

Summing up, there are three basic types of models:

- interface stability,
- concentration evolution with detailed reactions,
- simplified models with fixed geometry.

1.2 Applications

Briefly speaking, the main feature of nanotubular/nanoporous structure from the application point of view is its high specific surface area. This is obvious for any catalytic reaction. By diminishing dimensions to the nanoscale, not only the specific surface area increases significantly but also the electronic properties of these oxides may change considerably.

Among all transition-metal oxides, TiO_2 is the most extensively studied material. It is non-toxic, environmentally friendly, biocompatible and corrosion-resistant material. Titanium dioxide in all its crystal forms is a wide-bandgap semiconductor. It can be used for splitting water into oxygen and hydrogen, remediation of hazardous wastes (contaminated waters, toxic air contaminants) [Ghicov and Schmuki, 2009], [Grimes and Mor, 2009].

UV light promotes electrons from the valence band to the conduction band. Consequently, a semiconductor-environment interface is created and several highly

[3] Briefly speaking, it is an evolutionary equation $u_t + \nabla^4 u + \nabla^2 u + \frac{1}{2}|\nabla u|^2 = 0$ with partial time derivative, laplacian, biharmonic operator and gradient norm.

reactive species are formed from, e.g. surrounding water. These species are able to oxidise all organic material to CO_2 and H_2O. Apart from organic material decomposition holes from the valence band and electrons from the conduction band could react with H_2O to form H_2 and O_2. This light-induced catalytic mechanism is called *photocatalysis*.

2. Electrochemical model

2.1 Basic motivational experiment

It all begins with a real physical experiment. Our experimental setup is usually referred to as *electrochemical anodization cell*. It consists of electrolyte, (metal) electrodes and an outer voltage supply. A simple sketch of such cell is shown in Fig. 2.1. We will try to shortly explain the terms.

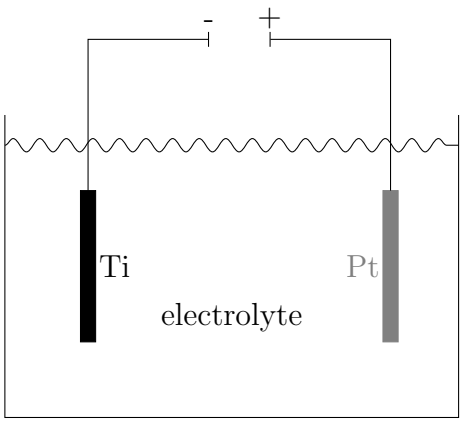

Figure 2.1: Sketch of a simple electrochemical cell.

Electrolyte is a substance, which becomes electrically conducting when dissolved into a polar solvent. Consider e.g. sodium chloride, NaCl dissolved in water. Solution as a whole stays electrically neutral, but sodium cations Na^+ and chloride anions Cl^- could migrate in an applied external electric field and facilitate the conduction mechanism.

In the scope of nanopores/nanotubes the electrolytes are composed of some small portion ($0.1-5$ % wt [1]) of $HF, HNO_3, H_3PO_4, NH_4F$ soluted in water. Some experimentalists use combination of these acids soluted in non-aqueous organic polar substances (ethylene glycol, dimethyl formamide...), see [Paulose et al., 2008].

Electrodes are pieces of metal sunk into the electrolyte. Minimal electrochemical cell involves two electrodes. Positive anode and negative cathode. When voltage of appropriate sign is applied, anode loses electrons as they move towards outer supply and cathode. We call this reaction *oxidation*. This partial point-of-view where we consider only one electrode with its surrounding electrolyte is called (electrochemical) *half-cell*.

In this thesis, only half-cell related to the anode is studied. We are interested in oxidation reaction which produces metal oxide. [2] If the anode is made of aluminum, Al_2O_3 is formed, if its made of titan, TiO_2 forms, etc.

[1] mass fraction percentage, i.e. mass of solute / (mass of solute + solvent) * 100

[2] Strictly speaking, it could happen, that no oxide is formed on the anode, for instance if electrolyte dissolves oxide rapidly. However, in this work we always assume some (at least nano-scale) oxide layer is present.

If we take a closer look at the surface of anode, we can distinguish three substances - metal, oxide and electrolyte, and their respective interfaces. Interface between metal and oxide will be abbreviated as MO interface and similarly for oxide electrolyte as OE interface. This zoomed picture is shown in Figure 2.2, and it will accompany us throughout whole thesis.

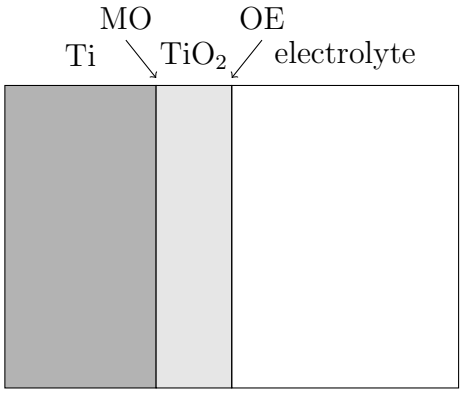

Figure 2.2: Closer look at half-cell for anode made of titan.

2.2 Thin layer growth, high-field conduction law

In the half-cell experiment, the metal anode gets covered with thin oxide layer.

Several models for the metal oxidation were developed. Early theories consider diffusion of uncharged/charged particles through the oxide film be the driving mechanism.

So called *Tammann Pilling Bedworth* theory is based on Fick's law of diffusion and predicts square root dependence of oxide thickness on time. Improvement in the form of *Wagner*'s theory considers electro-diffusion of charged particles.

However, when film thickness is in order of nanometers different mechanisms prevail. Most of the very thin film theories are based on [Cabrera and Mott, 1949].

Nice figure on validity of these theories is included, see Fig. 2.3. We can see there, that Cabrera & Mott theory is valid for thicknesses below, to some extent, say 1×10^{-7} m. This justifies our assumption, that metal oxidation in the geometry of nanopores/nanotubes (or in general in nanoscales) is governed by Cabrera & Mott theory. The same assumption is adopted in most of the papers on nanopores modeling, for instance [Parkhutik and Shershulsky, 1992, Cheng, 2015, Houser and Hebert, 2009, Hebert et al., 2012].

Their theory reveals mechanism that govern charged species transport through thin oxide layer. These mechanisms could be from macroscopic point of view seen as so called *high-field conduction law*. It is nothing but generalisation of well known linear Ohm law of conductivity for very high electric fields (approx. in order of volts per nanometers). According to [Houser and Hebert, 2009] high-field

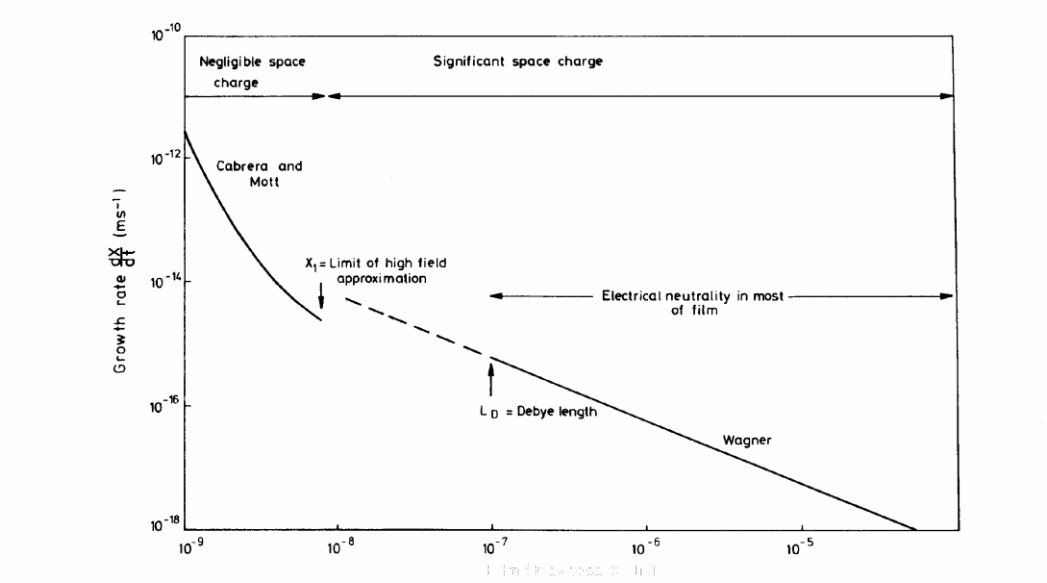

Figure 2.3: Validity of metal oxidation theories for various film thicknesses (in nm) for NiO.

Taken from [Fromhold Jr, 1976].

conduction law says

$$\boldsymbol{j}_i = -C_i u_i^0 \frac{\operatorname{grad}\bar{\phi}}{\left|\operatorname{grad}\bar{\phi}\right|} \sinh\left(\frac{z_i a F \left|\operatorname{grad}\bar{\phi}\right|}{RT}\right), \tag{2.1}$$

where $\boldsymbol{j}_i$ is the current density flux due to i-th ion in ampere per surface area, z_i is valence number of the moving ion, C_i concentration of the ion, u_i^0 is some pre-exponential referential ion velocity, $\bar{\phi}$ is electrostatic potential (the one which fulfils Maxwell electrostatic equations, it is denoted with upper bar, because there will be another electrostatic potential in this thesis), a is migration jump distance, R, T, F the gas constant, temperature and Faraday constant of electrolysis respectively. Their values are included in the results section.

One can define non-linear conductivity, $\sigma_o(\bar{\phi})$ [3], such that the differential form of the Ohm's law $\boldsymbol{j} = \sigma_o \boldsymbol{E} = -\sigma_o \operatorname{grad}\bar{\phi}$ is recognised. Simply with

$$\sigma_o := C_i u_i^0 \frac{1}{\left|\operatorname{grad}\bar{\phi}\right|} \sinh\left(\frac{z_i a F \left|\operatorname{grad}\bar{\phi}\right|}{RT}\right), \tag{2.2}$$

$$\boldsymbol{j}_i = -\sigma_{m,i} \operatorname{grad}\bar{\phi}. \tag{2.3}$$

It is called generalised Ohm law, because the current density is function of electric field in a form

$$\boldsymbol{j} = A \frac{\sinh\left(B\left|\operatorname{grad}\bar{\phi}\right|\right)}{\left|\operatorname{grad}\bar{\phi}\right|} \operatorname{grad}\phi \tag{2.4}$$

[3] We write the conductivity with lower index o to denote it is a conductivity of oxide layer. There will be conductivities of metal and electrolyte also, denoted σ_m, σ_e

which for low potential gradients (low electric field intensities) reduces to

$$\boldsymbol{j} \approx AB \operatorname{grad} \bar{\phi}, \qquad \text{for low electric fields,} \tag{2.5}$$

the well known Ohm law for conductivity AB. On the other hand, for very high electric fields, the $\sinh x = \frac{1}{2}(\exp x - \exp(-x)) \approx \frac{1}{2}\exp x$ so the high-field conduction is

$$\boldsymbol{j} \approx \frac{A}{2} \frac{\exp\left(B\left|\operatorname{grad} \bar{\phi}\right|\right)}{\left|\operatorname{grad} \bar{\phi}\right|} \operatorname{grad} \bar{\phi}, \qquad \text{for high electric fields.} \tag{2.6}$$

We have to make a comment on validity of the high-conduction law as stated here. The current density $\boldsymbol{j}_i$ is due to the flux of charged ions inside the oxide. Their flux is driven by the external electric field $\operatorname{grad} \bar{\phi}$. This is valid only if no concentration gradients of ions are present or the ions do not influence each other, e.g. they do not effect the external electric field. In terms of electrochemical potential we could say that the only difference in electrochemical potential between MO and OE interface is due to the electrostatic contribution. More on electrochemical potential in section 2.4.

Our quest is to start with some initial planar oxide layer thickness and let it grow - observe the dependence of its thickness on time. So far we know, that i-th specie is flowing (migrating) through thin oxide layer due to the high-field law (2.1). We need to sort out, what species are migrating. Then we can discuss how do each individual specie contributes to the interfacial (MO/OE) [4] movement.

Let us now think, for illustration, about the growth of TiO_2 layer. The simplest electrochemical picture is given in Figure 2.4.

According to the [Houser and Hebert, 2009] and many others, there are two types of species migrating within TiO_2. Oxide anions, O^{2-}, are supplied from *dissociation of the electrolyte* and from *dissolution of the* TiO_2 *layer.*

They migrate towards the metal, to the MO interface or react at OE interface. Titanium cations, Ti^{4+}, vacant after ionisation in the metal, form new oxide when they react with oxide anions. This reaction is written as

$$Ti^{4+} + 2\,O^{2-} \longrightarrow TiO_2. \tag{2.7}$$

It could happen at the MO interface or at OE interface.

In the Figure 2.4 possible reaction pathways are enumerated. Let us examine them:

① Ionised titanium cations meet oxide anions at OE interface. Oxide anions were supplied from dissolution of the oxide layer, so the remaining Ti^{4+} are ejected into electrolyte,

② titanium cations react at MO interface with oxide anions supplied from dissolution of oxide layer,

③ similar to ①, but the source of oxide anions is in dissociation of electrolyte,

④ similar to ②, but the source of oxide anions is in dissociation of electrolyte.

[4] Our MO/OE notation means, that the statement is valid for MO and/or OE interface.

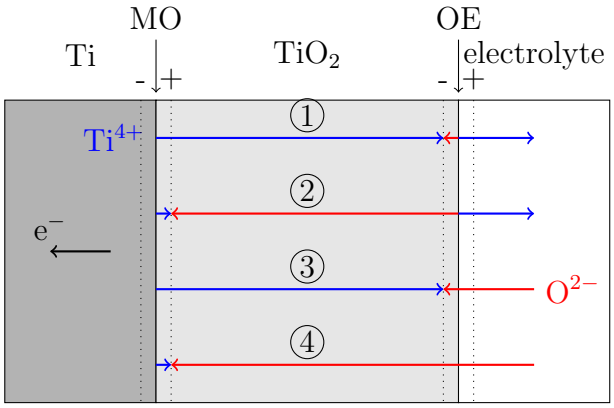

Figure 2.4: The simplest electrochemical picture.
There are Ti^{4+} (blue) and O^{2-} (red) ions reacting. This reaction forms new oxide, TiO_2, and it could take place somewhere at MO or at OE interface.

This picture tells us qualitatively, where do ions come from and where do we expect them to react. Nonetheless, quantitative description is a different question addressed in section 2.4.

We denoted total current density $\boldsymbol{j}$. There are several contributions to the total current density and these contributions vary from place to place, interface to interface. The current density $\boldsymbol{j}$ must have continuous normal component (we will discuss this later) but its contribution don't. Therefore, we have to be careful when talking about the "current at OE or MO" interface. We must specify which side of OE/MO is actually thought of.

Because we denoted the interfaces as OE and MO, ordering of letters naturally define some orientation of the interface. OE means oxide to electrolyte, so the natural orientation of normal would be pointing outside of the oxide, to the electrolyte. If we write $\boldsymbol{j}^{\mathrm{OE}+}_{\mathrm{O}^{2-}}$ then we mean current due to O^{2-} inside electrolyte, right next to the OE interface. Writing $\boldsymbol{j}^{\mathrm{OE}-}_{\mathrm{O}^{2-}}$ current inside oxide is meant. If no sign is denoted then the partial current has continuous component and both limits are equal. Orientations of the interfaces are depicted in Figure 2.4 with dotted lines.

2.3 Total current density and current continuity

Current density due to the flux of i-th ion is denoted $\boldsymbol{j}_i$. If there are several ions flowing then total current density, i.e. flux of total charge could be written as

$$\boldsymbol{j} = \sum_{i \in \text{ions}} \boldsymbol{j}_i. \tag{2.8}$$

Let us define a charge density ρ.

In terms of physics it is a limit of total charge contained inside some volume $\mathcal{V}$ divided by measure of this volume $|\mathcal{V}|$ as this measure approaches zero, i.e. $\rho = \lim_{|\mathcal{V}|\to 0} Q(\mathcal{V})/|\mathcal{V}|$.

In terms of mathematics, the charge measure is absolutely continuous with respect to the volume measure and therefore due to the *Radon-Nikodym* theorem,

see [Rudin, 1987] (Theorem 6.10), there exists an L^1 function called charge density ρ.

Having defined the charge density, let us write the law of conservation of total charge for a fixed (no advection term) test volume in differential form. It states

$$\frac{\partial \rho}{\partial t} = -\operatorname{div} \boldsymbol{j}, \tag{2.9}$$

where $\boldsymbol{j}$ is the flux of the charge density here. It is by the definition the same quantity as the total current density.

If we assume there is no region, where total charge density is being accumulated/removed, then

$$\frac{\partial \rho}{\partial t} = 0 \quad \Rightarrow \quad \operatorname{div} \boldsymbol{j} = 0. \tag{2.10}$$

Total current density is divergence free. This equation is the most basic equation in this thesis. We will refer to this equation as to the *current continuity equation*. Total current density will have different forms and different boundary conditions will be applied, but the structure of this equation will be preserved.

2.4 Butler-Volmer kinetic relation

We will follow the book [Newman and Thomas-Alyea, 2012].

One of the simplest relation between current density j and *surface overpotential* η_s is so called *Butler-Volmer* equation

$$\boldsymbol{j} \cdot \boldsymbol{n} = i_0 \left[\exp\left(\frac{\alpha_a F}{RT} \eta_s \right) - \exp\left(-\frac{\alpha_c F}{RT} \eta_s \right) \right] \tag{2.11}$$

where i_0, α_a and α_c are kinetic parameters, namely the *exchange current density*, anodic and cathodic *transfer coefficients*. The parameter i_0 depends on the composition of the solution adjacent to the electrode, temperature and nature of the electrode surface. More difficult is to define the surface overpotential η_s. Let us quote the [Newman and Thomas-Alyea, 2012]:

"Much of the electrochemical literature is written in terms of electrical potentials of various kinds, and it is necessary to set our minds straight on these matters and to investigate how potentials might be used in electrochemistry. **Much of the confusion in electrochemistry arises from uncertainty in the use of these concepts.**"

If we say potential or cell potential we mean the difference of *electrochemical potentials* of electrons between the electrodes divided by Faraday's constant. We will denote different types of potentials (not electrochemical!) with Φ and they will always refer to some value, which could be measured with a voltmeter.

The electrochemical potential is a thermodynamic quantity which measures how the internal energy changes when a substance is added/removed. In contrast to pure chemical potential it does not omit the energy contribution by electrostatics but it incorporates the electrostatic energy and the influence of electric field on intermolecular forces.

Overpotential, in general sense, refers to the magnitude of a potential drop caused by resistance to the passage of current. Potentials could be measured

only with respect to some reference state. In physics, the reference state is a potential of an electron in a vacuum (infinitely far away), electrochemists use *reference electrode*, an electrode designed so that its potential is well-defined and reproducible. Let us revisit the Figure 2.1 and add reference electrode into it. This setup is shown in Figure 2.5.

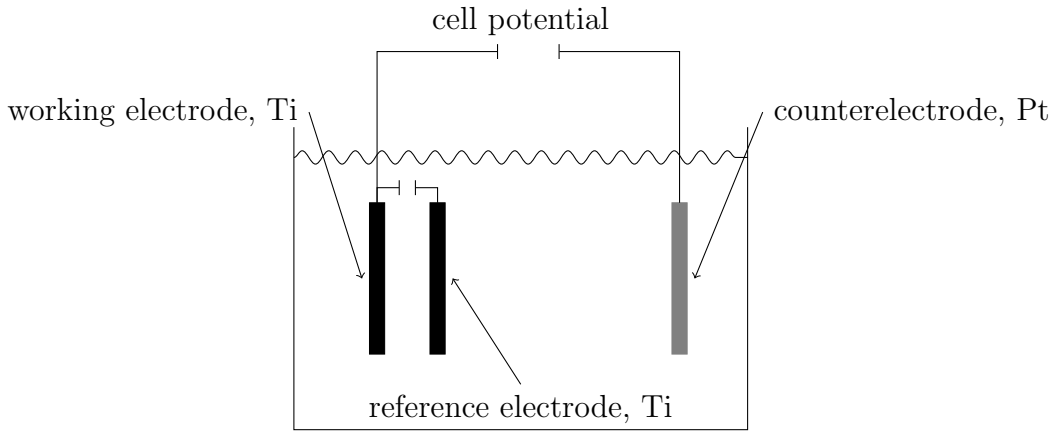

Figure 2.5: Sketch of a simple electrochemical cell with the electrodes added.

A potential measured on high impedance [5] voltmeter between working and counterelectrode is called *cell potential*. It is basically an overall potential consisting of several contributions and drops within the whole electrochemical cell.

A potential measured on high impedance voltmeter between working and reference electrode of the same (!) material, surface roughness, temperature, pressure, etc. is called the *surface overpotential*. It is very important that the reference electrode is made of the same material, with the same temperature, surface properties, etc. Due to the different thermodynamic nature of the electrolyte and metal electrode there always exists some (electrochemical) potential jump on their interface. It is caused simply because the electrons have different electrochemical potential in metal and in electrolyte. They flow to the more favourable environment and this flow is measured with a voltmeter as a potential difference. If we use reference electrode with the same properties then these contributions to the potential difference cancel and we see only the pure surface overpotential.

The overall (cell) overpotential is caused by several types of resistances to a current. The surface overpotential represents the resistance due to electrochemical reaction[6], *ohmic overpotential* represents the resistance to ionic or electronic current and *concentration overpotetial* accounts for concentration gradients causing the potential drop.

In order to complete our picture we have to define the last source of potential difference in electrochemical cell. If we place piece of tarnished silver into salt water electrolyte and connects it with zinc, the silver will become shiny and zinc will dissolve. It is the thermodynamic properties of silver, silver oxide, zinc, and zinc oxide that determine that silver oxide is reduced spontaneously at the expense

[5] So negligible current flows through voltmeter.

[6] Electrochemical reaction has some inner rate at which it is advancing. This is exactly the relation (2.11).

of zinc. The current flowing between silver and zinc electrode won't be zero. We already discussed the reasons for this current (difference in electrochemical potentials in different materials in contact). This could be easily measured. We can connect electrodes to a *potentiostat* and adjust the potential difference to some value when no current is flowing. This value of potential is called *equilibrium* or *open-circuit potential*.

Our interest is not in full electrochemical cell as in Figure 2.5 but rather the zoomed-in half cell, as in 2.2. The terminology and theory described in this section could be used also in the half-cell case.

As depicted in Figure 2.6, imagine metal covered with an oxide layer and surrounded with an electrolyte. If we were able to construct electrode of the same material as the metal and place it close to the MO interface [7], into the oxide, and we were able to measure the potential difference between these "electrodes" we would measure the surface overpotential for the MO interface, $\eta_{\mathrm{s,MO}}$. Similar idea leads to the surface overpotential for the OE interface, $\eta_{\mathrm{s,OE}}$. These overpotentials are related to the currents passing through MO/OE interfaces via (2.11).

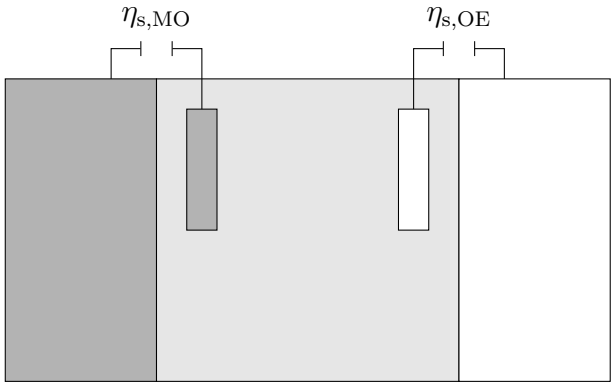

Figure 2.6: Electrochemical picture of the anode half-cell with probe electrodes.

The potential distribution is shown in Figure 2.7.

Blue dash-dotted line represents the potential distribution when no outer potentiostat is connected. The only potential jump is due to the open-circuit potential, i.e. the different thermodynamic nature of metal, oxide and electrolyte. These open-circuit potentials are denoted U_{MO} and U_{OE}.

If we now connect a potentiostat and apply a potential Φ_0 we change the distribution as shown with red solid line. Both potential jumps (overpotentials) are increased with additional contributions. The surface overpotentials that were virtually measured in Figure 2.7 represent the inner resistance of the chemical reactions to the outer driving potential.

We should not forget, that the ohmic drop inside the oxide layer (the sloped lines in Figure 2.7) is determined by the high-conduction law as discussed in section 2.2.

[7] This is of course impossible. Physical dimensions of the oxide layer are in order of nanometres, oxide is moreover a solid substance.

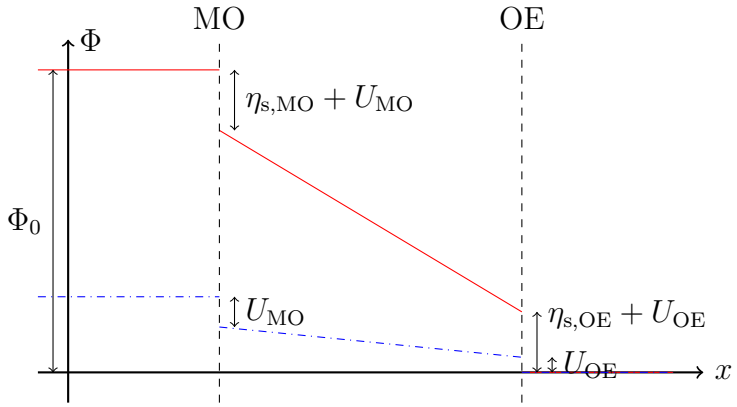

Figure 2.7: Potential distribution in our electrochemical picture.

2.5 Faraday's law of electrolysis and interface evolution

Once the current passing through interface is known we have to evolve it. Faraday's law of electrolysis is nothing, but balance of mass and charge for charged species reacting at an interface. It states

$$m = \frac{QM}{zF}, \tag{2.12}$$

where m is mass of substance liberated/deposited in kilograms, Q is total charge passed through interface in coulombs, M is the molar mass of the substance in kilograms per mole, $F = 96\,485.332\,\mathrm{C\,mol^{-1}}$ the Faraday's constant with the meaning of electric charge per mole of electrons and z being the valency number of ions of the substance, i.e. electrons transferred per ion.

Illustration of reacting ions is in Figure 2.8.

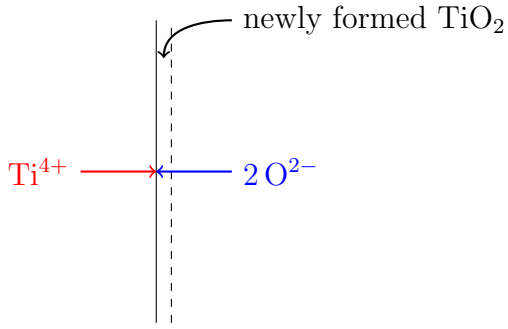

Figure 2.8: Illustration of the Faraday's law of electrolysis.
The charge of 4 electrons is being transported.

It is often more useful to use the law in differential form. For the simple derivation of differential form divide the equation (2.12) with some small time

step Δt and some small surface area, ΔS to get

$$\frac{m}{\Delta t \Delta S} = \frac{Q}{\Delta t \Delta S}\frac{M}{zF} = j\frac{M}{zF} = \frac{\Delta d \Delta S \rho}{\Delta t \Delta S} = \rho\frac{\Delta d}{\Delta t}. \tag{2.13}$$

Where j is the current density in coulomb per second per metre squared, Δd is thickness of newly formed planar(!) oxide layer in metres and ρ its density in kilograms per metres cubed. Letting $\Delta t, \Delta S \longrightarrow 0$ we have the differential form

$$\frac{\mathrm{d}}{\mathrm{d}t}d(t) = j\frac{M}{z\rho F} \tag{2.14}$$

For the specific case of titanium dioxide $z = 4$ and

$$\frac{\mathrm{d}}{\mathrm{d}t}d(t) = j\frac{M_{\mathrm{TiO_2}}}{4\rho_{\mathrm{TiO_2}}F} \tag{2.15}$$

It was experimentally observed, that if we let the anodic oxidation happen, the new oxide grows on both interfaces, MO and OE. However it does not grow on both interfaces equally fast. Ratio of the speed of the growth of interfaces could be measured in "simple" experiment. It is illustrated in Figure 2.9.

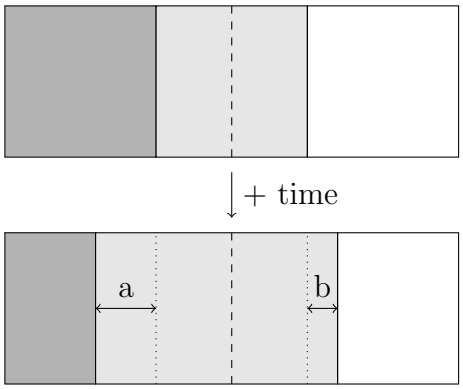

Figure 2.9: An illustation of the transport number, t_O.

Let newly grown oxide layers at MO and OE interfaces have thickness a and b respectively. We can define ratio

$$r = \frac{a}{a+b}$$

which express, what fraction of newly grown oxide (on both interfaces) was grown at MO interface.

Let us, in addition, define a number, $t_O \in [0, 1]$, we will call it *transport number of the oxygen ions*. This number express what fraction of oxide anion current $\boldsymbol{j}^{\mathrm{OE}-}_{\mathrm{O}^{2-}}$ is transported from OE to the MO interface. In the virtue of Figure 2.4 it is a ratio between current of O^{2-} (red) due to the ② + ④ and the total current density $\boldsymbol{j}^{\mathrm{OE}} \cdot \boldsymbol{n}$. This number is usually stated in the papers on thin layer oxide growth, see for example [Houser and Hebert, 2006]. Symbolically we write

$$t_O = \frac{② + ④}{\boldsymbol{j}^{\mathrm{OE}} \cdot \boldsymbol{n}}. \tag{2.16}$$

Natural question arises: what is the connection between both defined numbers, t_O and r? The only way, how MO interface can grow is due to incoming oxide anions, ② + ④. The thickness a is therefore proportional to this current with some faradaic constant, say C. This constant depends on mass and density of oxide that is formed. On the other hand, the total thickness $a+b$ is proportional to the total current density $\boldsymbol{j}^{\mathrm{OE}} \cdot \boldsymbol{n}$ with the same constant C, because we assume that the oxide with the same material properties is growing (and dissolving). We can therefore write

$$r = \frac{a}{a+b} = \frac{C(② + ④)}{C\boldsymbol{j}^{\mathrm{OE}} \cdot \boldsymbol{n}} = \frac{② + ④}{\boldsymbol{j}^{\mathrm{OE}} \cdot \boldsymbol{n}} = t_O.$$

In other words, transport number and number r are both equal and express how fast is growing MO interface comparing to how fast is growing OE interface.

We are now few steps from the formulation of how the thickness of oxide film grows for given total current density, $\boldsymbol{j}$. The last thing we need is so called *oxide current efficiency*, denoted usually ε. Again, from our basic electrochemical picture (Figure 2.4), total current density at OE+ [8] interface is due to flux of oxide anions from dissociation in electrolyte and due to flux of ionised titanium cations that come from MO interface. We can write

$$\boldsymbol{j}^{\mathrm{OE+}} = \boldsymbol{j}^{\mathrm{OE+}}_{\mathrm{O}^{2-}} + \boldsymbol{j}^{\mathrm{OE+}}_{\mathrm{Ti}^{4+}}.$$

The oxide current efficiency is defined as

$$\varepsilon := \frac{\boldsymbol{j}^{\mathrm{OE+}}_{\mathrm{O}^{2-}} \cdot \boldsymbol{n}}{\boldsymbol{j}^{\mathrm{OE+}}_{\mathrm{O}^{2-}} \cdot \boldsymbol{n} + \boldsymbol{j}^{\mathrm{OE+}}_{\mathrm{Ti}^{4+}} \cdot \boldsymbol{n}} = \frac{\boldsymbol{j}^{\mathrm{OE+}}_{\mathrm{O}^{2-}} \cdot \boldsymbol{n}}{\boldsymbol{j}^{\mathrm{OE+}} \cdot \boldsymbol{n}}. \tag{2.17}$$

In other words, it is the ratio between the oxide anion current and the total current density at OE interface.

Following the [Houser and Hebert, 2006] we will write the interface evolution based on the oxide anion balance.

The OE interface evolution [9] is based on two contributions:

- negative contribution (growth of new layer). Oxide anions from dissociation of electrolyte react at OE interface and create new oxide, pathway ③,
- positive contribution (layers being dissolved). The TiO_2 is dissolved and arosed oxide anions are transported to MO interface, pathway ②.

Symbolically

$$\boldsymbol{v}_{\mathrm{OE}} \cdot \boldsymbol{n} = C(② + ③).$$

We can express the pathway ③ with the help of current efficiency as

$$③ = \varepsilon \boldsymbol{j}^{\mathrm{OE+}} - ④$$

[8] The (normal component of) total current density is continuous through interfaces, the plus sign here is not necessary. However, decomposition of the total current density at OE+ side is more simple, comparing to decomposition of the total current density at OE− side.

[9] Our sign convention is, that positive interfacial speed means removal rate, i.e. the layer is dissolved. Negative interfacial speed means addition of new layers.

since oxide anion current at OE+ interface is by the definition of current efficiency equal to $\varepsilon \boldsymbol{j}^{\mathrm{OE+}}$ (red lines in electrolyte in Figure 2.4) and we subtracted the pathway ④. With the help of this we can write OE speed as

$$\begin{aligned}\boldsymbol{v}_{\mathrm{OE}} \cdot \boldsymbol{n} &= C(② + ③) = C(② + ④) - C\varepsilon \boldsymbol{j}^{\mathrm{OE+}} = C(t_O \boldsymbol{j}^{\mathrm{OE}} - \varepsilon \boldsymbol{j}^{\mathrm{OE+}}) = \\ &= (t_O - \varepsilon)\boldsymbol{j}^{\mathrm{OE}} \cdot \boldsymbol{n} \frac{M_{\mathrm{TiO_2}}}{4\rho_{\mathrm{TiO_2}} F} \end{aligned} \tag{2.18}$$

where definition of transport number was used and actual values of constant was taken from Faraday's law of electrolysis (2.15).

The first term on the right hand side in previous relation is the removal rate due to transport to MO interface, while the second term is growth rate due to O^{2-} dissociated in electrolyte.

The MO interface cannot dissolve (in this model), so the only mechanism which evolve the interface is due to oxidation reaction of oxide anions that are transported from OE interface. We can write Faraday's law as

$$\boldsymbol{v}_{\mathrm{MO}} \cdot \boldsymbol{n} = t_O \boldsymbol{j}^{\mathrm{MO}} \cdot \boldsymbol{n} \frac{M_{\mathrm{TiO_2}}}{4\rho_{\mathrm{TiO_2}} F}. \tag{2.19}$$

The equations (2.18) and (2.19) are very important. They substantially influence the growth process. However, it is hard to imagine how the model behaves for different values of t_O and ε. Let us examine some simple cases.

- Take $t_O = 1$ and $\varepsilon = 0$. It means, that all of the O^{2-} migrates towards MO and no O^{2-} is supplied from electrolyte. They must therefore come from dissolution of $\mathrm{TiO_2}$. The OE interface is for given $\boldsymbol{j}^{\mathrm{OE}}$ advancing with maximal possible speed towards MO. But MO is also moving with maximal speed, since each O^{2-} is transfered to MO interface where it forms the oxide.

- Take $t_O = 0$ and $\varepsilon = 1$. No oxide ion migrates through oxide layer and all of the current is due to formation in electrolyte. We can simply see, that OE would advance in opposite direction as the previous case and MO interface would not move at all. In other words, the oxide thickness increases.

- In general, whenever $t_O = \varepsilon$ the OE interface is not moving. Why? Because each oxide ion which is supplied from water is transported through oxide layer and vice versa, each oxide which is transported is the one, which was formed in water.

Transport number for oxide anions is usually measured and given from some experiments. Most of the literature consider transport number to be constant. On the other hand, the oxide current efficiency, ε, changes substantially. It is a result of chemical reactions and their mutual competition. Any time there are some electrochemical reactions they influence the current density as Butler-Volmer relation suggests. Because the oxide anion current density at OE+ interface is a result of some processes (dissociation) in electrolyte we can write Butler-Volmer relation in form (2.11)

$$\boldsymbol{j}^{\mathrm{OE+}}_{\mathrm{O^{2-}}} \cdot \boldsymbol{n} = i_{0,\mathrm{O^{2-}}} \left[\exp\left(\frac{\alpha_{a,\mathrm{O^{2-}}} F}{RT} \eta_{s,\mathrm{OE}} \right) - \exp\left(-\frac{\alpha_{c,\mathrm{O^{2-}}} F}{RT} \eta_{s,\mathrm{OE}} \right) \right], \tag{2.20}$$

where $i_{0,\mathrm{O}^{2-}}, \alpha_{a,\mathrm{O}^{2-}}, \alpha_{c,\mathrm{O}^{2-}}$ are kinetic coefficients related to the reactions at OE interface and $\eta_{s,\mathrm{OE}}$ is our well known surface overpotenial at OE interface defined in previous sections.

Titanium cation current density (at OE interface) is also a result of some electric field induced effects and is here modelled as

$$\boldsymbol{j}^{\mathrm{OE}+}_{\mathrm{Ti}^{4+}} \cdot \boldsymbol{n} = i_{0,\mathrm{Ti}^{4+}} \left[\exp\left(\frac{\alpha_{a,\mathrm{Ti}^{4+}} F}{RT} \eta_{s,\mathrm{OE}} \right) \right], \tag{2.21}$$

where again, $i_{0,\mathrm{O}^{2-}}, \alpha_{a,\mathrm{O}^{2-}}$ are kinetic coefficients related to reactions at OE in which Ti^{4+} participate. Note, that current density for titanium cations doesn't contain cathodic (negative) exponential term. This engender that for $\eta_{s,\mathrm{OE}} = 0$ we have $\boldsymbol{j}^{\mathrm{OE}+}_{\mathrm{Ti}^{4+}} \cdot \boldsymbol{n} \neq 0$. This assumption of nonzero titanium current even for zero overpotential is in agreement with experimental data from [Vetter and Gorn, 1973].

Summing up - if we are given the transport number t_O, surface overpotential $\eta_{s,\mathrm{OE}}$ and total current density $\boldsymbol{j}$ we can compute from (2.20), (2.21) and (2.17) the current efficiency. Plugging into (2.18) gives the OE interface evolution. Similar procedure applies also for the MO interface.

We are now finally able to provide an overall picture for the electrochemical theory of thin layer oxide growth in the following section.

2.6 Overall picture

Overall picture consists of several steps and physical mechanisms.

① Identify ions migrating through the oxide layer. For the case of TiO_2 these are Ti^{4+} and O^{2-}.

② In order to find generalised conductivities $\sigma_{o,i}(\bar{\phi})$ we need to find the electrostatic potential $\tilde{\phi}$. From the high-field conduction law (2.1) and current continuity (2.10) we have

$$\operatorname{div} \boldsymbol{j} = \operatorname{div}\left(\sum_{i \in \mathrm{ions}} \boldsymbol{j}_i \right) = \operatorname{div}\left(\sum_{i \in \mathrm{ions}} C_i u_i^0 \frac{\operatorname{grad} \bar{\phi}}{\left|\operatorname{grad} \bar{\phi}\right|} \sinh\left(\frac{z_i a F \left|\operatorname{grad} \bar{\phi}\right|}{RT} \right) \right) = 0, \tag{2.22}$$

which is a highly non-linear second order elliptic partial differential equation in an unknown quantity, potential $\bar{\phi}$.

③ Electrochemical reaction at the interfaces must be incorporated. This is governed with the boundary conditions such as (2.11). They couple jumps in potential at the interfaces ($[[\phi]]_{\mathrm{MO}} = \eta_{\mathrm{s,MO}} + U_{\mathrm{MO}}, [[\phi]]_{\mathrm{OE}} = \eta_{\mathrm{s,OE}} + U_{\mathrm{OE}}$) with normal component of total current density. We have to find a potential and total current density, such that jump conditions as in Figure 2.7 are satisfied and such that the potential fulfils ② inside the oxide domain. Conductivities in metal and electrolyte are assumed constant and given numbers, say σ_m, σ_e.

This is a task of solving mixed system of equations and finding $\boldsymbol{j}, \phi$ satisfying

$$\operatorname{div} \boldsymbol{j} = 0, \tag{2.23}$$

$$\boldsymbol{j} = -\sigma \operatorname{grad} \phi \tag{2.24}$$

with conductivity constant σ_m in metal, $\sigma_o(\phi)$ in oxide (varying in space) and constant σ_e in electrolyte. We denoted this potential ϕ (without bar!) because it is different function from potential from the step ②, $\bar{\phi}$. Potential ϕ is defined everywhere in metal, oxide and electrolyte and satisfies the Butler-Volmer jump conditions. On the other hand, the potential $\bar{\phi}$ is used solely to compute the non-linear conductivity of oxide, i.e. $\sigma_{o,i}(\bar{\phi})$. The reason why the mixed system must be solved will become clear in following mathematical chapters and is related to the jumps in solution, ϕ.

④ Having total current density $\boldsymbol{j}$ and overpotentials (jumps) computed from step ③ we could plug into relations (2.18) and (2.19) to get production rates. These are used to evolve the geometry of our problem and we could start from the step ② again.

3. Mathematical model

After describing the electrochemical model in the previous chapter, we could step into more rigorous, mathematical formulation of the equations. In the beginning of this chapter high-field conduction is formulated, followed by mixed formulation which incorporates jumps in electrostatic potential. In the end, time is added to our formulation and reaction equations evolving the interfaces are given.

Each section of this chapter formulates problem on the same bounded domain (=open, connected), $\Omega \subset \mathbb{R}^d, d \in \mathbb{N}, d \geq 1$ of class $\mathrm{C}^{0,1}$. Let Γ be its Lipschitz continuous boundary. Let Γ_D and Γ_N be disjoint parts of Γ such that $|\Gamma_D| \neq 0$ and $\overline{\Gamma} = \overline{\Gamma_D} \cup \overline{\Gamma_N}$.

Moreover let us define $\Omega_m(t), \Omega_o(t), \Omega_e(t) \subset \Omega$ such that $\overline{\Omega} = \overline{\Omega_m(t)} \cup \overline{\Omega_o(t)} \cup \overline{\Omega_e(t)}$ and each subdomain have Lipschitz-continuous boundary (they evolve in time, so regularity of domain depends on a way, how their time evolution is defined). The time $t \in I := [0, T]$. Additionaly, there are interfaces, let us call them $\Gamma_{\mathrm{MO}}(t) := \partial\Omega_m(t) \cap \partial\Omega_o(t)$ and $\Gamma_{\mathrm{OE}}(t) := \partial\Omega_o(t) \cap \partial\Omega_e(t)$.

We also require $\Gamma_{\mathrm{MO}}(t) \cap \Gamma_D = \Gamma_{\mathrm{OE}}(t) \cap \Gamma_D = \emptyset$ and $\boldsymbol{n}_{\Gamma_{\mathrm{MO}}}(t) \cdot \boldsymbol{n}_{\Gamma_N} = \boldsymbol{n}_{\Gamma_{\mathrm{OE}}}(t) \cdot \boldsymbol{n}_{\Gamma_N} = 0$ where both are defined. [1]

An example of such domain Ω with its boundaries and interfaces is shown in Figure 3.1.

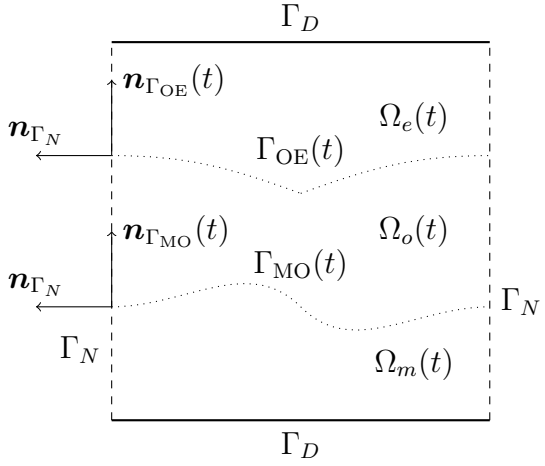

Figure 3.1: An example of Ω.
Dirichlet boundaries are shown with solid line, Neumann boundaries with dashed line and the interface is shown with dotted line.

[1] The first condition assures, that we do not need to care about compatibility of boundary data prescribed at Γ_D and jump condition prescribed at $\Gamma_{\mathrm{MO/OE}}(t)$.

The second condition is less trivial. If a jump in ϕ is prescribed on a surface which is not perpendicular to the boundary, then normal derivative of ϕ has some non-zero component in direction $\boldsymbol{n}_{\Gamma_N}$. This component should be also compatible with Neumann data prescribed on Γ_N. We again do not want to bother with compatibility conditions for this, so perpendicular interface is chosen.

Bear in mind, that interface changes in time so it could happen $\boldsymbol{n}_{\Gamma_{\mathrm{MO}}}(t) \cdot \boldsymbol{n}_{\Gamma_N} \neq 0$. It is necessary to enforce this condition in some post-processing step.

The Figure 3.1 is nothing but our half-cell from previous chapter, 2.2, rotated 90 degrees counter-clockwise. Recall it's composition from metal (Ti or Ω_m), oxide (TiO_2 or Ω_o) and electrolyte (Ω_e).

In the following, several mathematical equations are formulated on the same domain Ω.

3.1 High-field conduction law

Electrochemical motivation for this equation is summarised in Section 2.6, point ②. Weak formulation for the equation (2.22) reads: find $\bar{\phi} \in V$ such that

$$\left(\sigma \operatorname{grad} \bar{\phi}, \operatorname{grad} v\right)_{\mathrm{L}^2(\Omega)} = 0 \tag{3.1}$$

for all $v \in V$ where

$$\sigma = \sigma_m \quad \text{in } \Omega_m(t),$$

$$\sigma = \sigma_o(\bar{\phi}) := \sum_{i \in \text{ions}} C_i u_i^0 \frac{1}{\left|\operatorname{grad} \bar{\phi}\right|} \sinh\left(\frac{z_i a F \left|\operatorname{grad} \bar{\phi}\right|}{RT}\right) \quad \text{in } \Omega_o(t),$$

$$\sigma = \sigma_e \quad \text{in } \Omega_e(t),$$

$$V := \{v \in \mathrm{H}^1(\Omega); v = 0 \text{ on } \Gamma_D \text{ in the sense of trace}\}.$$

This high-field potential fulfils homogeneous Dirichlet boundary conditions, but application of prescribed boundary conditions, say ϕ_0 on Γ_D is treated in a classical way.

3.2 Mixed formulation for discontinuous solution

3.2.1 Problem definition

Electrochemical motivation for this equation is summarised in Section 2.6, point ③. We would like to find a potential ϕ which is not continuous at the MO and OE interfaces. Clearly, it is not possible to look for ϕ satisfying $-\Delta\phi = 0$ in classical sense. Additionally, for a weak formulation we would need $(\operatorname{grad}\phi, \operatorname{grad} v)_{\mathrm{L}^2(\Omega)}$, but it is not possible to interpret $\operatorname{grad}\phi$ either without a notion of distributions.

We could formulate our problem in a piecewise sense find $\phi : \Omega \longrightarrow \mathbb{R}$ such that

$$-\operatorname{div}(\sigma_m \operatorname{grad}\phi) = 0 \quad \text{in} \quad \Omega_m(t), \tag{3.2}$$

$$-\operatorname{div}(\sigma_o(\bar{\phi}) \operatorname{grad}\phi) = 0 \quad \text{in} \quad \Omega_o(t), \tag{3.3}$$

$$-\operatorname{div}(\sigma_e \operatorname{grad}\phi) = 0 \quad \text{in} \quad \Omega_e(t), \tag{3.4}$$

$$\phi = f \quad \text{on} \quad \Gamma_D, \tag{3.5}$$

$$-\sigma \operatorname{grad}\phi \cdot \boldsymbol{n}_{\Gamma_N} = 0 \quad \text{on} \quad \Gamma_N, \tag{3.6}$$

$$[[-\sigma \operatorname{grad}\phi \cdot \boldsymbol{n}_{\Gamma_{\mathrm{MO}}}(t)]] = 0 \quad \text{on} \quad \Gamma_{\mathrm{MO}}(t), \tag{3.7}$$

$$[[-\sigma \operatorname{grad}\phi \cdot \boldsymbol{n}_{\Gamma_{\mathrm{OE}}}(t)]] = 0 \quad \text{on} \quad \Gamma_{\mathrm{OE}}(t), \tag{3.8}$$

$$[[\phi]] = g_{\mathrm{MO}}(-\sigma \operatorname{grad}\phi \cdot \boldsymbol{n}_{\Gamma_{\mathrm{MO}}}(t)) \quad \text{on} \quad \Gamma_{\mathrm{MO}}(t), \tag{3.9}$$

$$[[\phi]] = g_{\mathrm{OE}}(-\sigma \operatorname{grad}\phi \cdot \boldsymbol{n}_{\Gamma_{\mathrm{OE}}}(t)) \quad \text{on} \quad \Gamma_{\mathrm{OE}}(t). \tag{3.10}$$

Function

$$\sigma = \begin{cases} \sigma_m & \text{if } \boldsymbol{x} \in \Omega_m(t), \\ \sigma_o(\bar{\phi}) & \text{if } \boldsymbol{x} \in \Omega_o(t), \\ \sigma_e & \text{if } \boldsymbol{x} \in \Omega_e(t). \end{cases}$$

Functions g_{MO} and g_{OE} are inverted Butler-Volmer relations (2.11). More specifically, Butler-Volmer relations couple surface overpotential with current density normal component. If we neglect the open-circuits potential (the constant contributions to the jump at the interface, $U_{\mathrm{MO/OE}}$) we can find $\boldsymbol{j} \cdot \boldsymbol{n} = g_{\mathrm{MO/OE}}(\eta_s) = g_{\mathrm{MO/OE}}([[\phi]])$.

The $[[\phi]]$ denotes a jump in a function ϕ defined as $[[\phi]] := \phi^+ - \phi^-$ with ϕ^+ and ϕ^- being one-side limits, i.e. $\phi^{+/-}(\boldsymbol{x}) := \lim_{\varepsilon \to 0^{+/-}} \phi(\boldsymbol{x} + \varepsilon \boldsymbol{n}_{\Gamma_{\mathrm{MO/OE}}})$.

3.2.2 Weak solution

An idea of a proper mixed weak solution will be derived. For that reason let us suppose that functions $\phi, \sigma_m, \sigma_o(\phi), \sigma_e, f, g_{\mathrm{MO,OE}}$ are sufficiently smooth.

For simplicity, we will derive a proper formulation neglecting Ω_e, i.e. assuming only a jump at MO interface. Additional jump condition will be added in a similar way.

As usual in mixed formulation, define additional quantity

$$\boldsymbol{j} := -\sigma \operatorname{grad} \phi \quad \text{in} \quad \Omega_m(t) \cup \Omega_o(t).$$

With the aid of this quantity equations (3.6), (3.9) become

$$\boldsymbol{j} \cdot \boldsymbol{n}_{\Gamma_N} = 0 \qquad \text{on} \quad \Gamma_N, \tag{3.11}$$

$$[[\phi]] = g_{\mathrm{MO}}(\boldsymbol{j} \cdot \boldsymbol{n}_{\Gamma_{\mathrm{MO}}}) \quad \text{on} \quad \Gamma_{\mathrm{MO}}(t). \tag{3.12}$$

Multiply equations (3.2), (3.3) with arbitrary test function $v \in \mathrm{C}_c^\infty(\Omega)$, integrate over $\Omega_m(t), \Omega_o(t)$ and sum together leading to

$$\int\limits_{\Omega_m(t) \cup \Omega_o(t)} (\operatorname{div} \boldsymbol{j}) v \, \mathrm{d}x = 0. \tag{3.13}$$

In a similar fashion, multiply the definition of $\boldsymbol{j}$ (3.11) with another arbitrary test function $\boldsymbol{\tau} \in \{\boldsymbol{f}; \boldsymbol{f} \in (\mathrm{C}^\infty(\overline{\Omega}))^d; \boldsymbol{f} \cdot \boldsymbol{n}_{\Gamma_N} = 0\}$ and integrate over $\Omega_m(t), \Omega_o(t)$ to get

$$\int\limits_{\Omega_m(t) \cup \Omega_o(t)} \boldsymbol{j} \cdot \boldsymbol{\tau} \, \mathrm{d}x - \int\limits_{\Omega_m(t)} (-\sigma \operatorname{grad} \phi) \cdot \boldsymbol{\tau} \, \mathrm{d}x - \int\limits_{\Omega_o(t)} (-\sigma \operatorname{grad} \phi) \cdot \boldsymbol{\tau} \, \mathrm{d}x = 0.$$

It was not specified yet, but naturally $\sigma \neq 0$ [2] in Ω and we divide by it. Moreover, according to courageous assumptions on ϕ we can use Green's identity

[2] This condition it not so trivial. Recall, that σ inside the oxide domain is given from the previous solution $\bar{\phi}$ to the high-field conduction law. Inside metal domain we are fine, since it is set to a given non-zero constant. Inside oxide domain we can see, that it is in the form $\sinh(x)/x$. This function has image $[1, +\infty]$, so lower bound is easily found.

and arrive at

$$\int_{\Omega} \sigma^{-1}\boldsymbol{j}\cdot\boldsymbol{\tau}\,\mathrm{d}x - \int_{\Omega_m(t)\cup\Omega_o(t)} \phi\,\mathrm{div}\,\boldsymbol{\tau}\,\mathrm{d}x + \int_{\partial\Omega_m(t)} \phi\boldsymbol{\tau}\cdot\boldsymbol{n}_{\partial\Omega_m(t)}\,\mathrm{d}S + \int_{\partial\Omega_o(t)} \phi\boldsymbol{\tau}\cdot\boldsymbol{n}_{\partial\Omega_o(t)}\,\mathrm{d}S = 0.$$

The boundaries $\partial\Omega_m(t)\cup\partial\Omega_o(t) = \partial(\overline{\Omega_m(t)\cup\Omega_o(t)}) + \Gamma_{\mathrm{MO}}(t) - \Gamma_{\mathrm{MO}}(t)$ where minus sign formally represents the opposite orientation. The test functions $\boldsymbol{\tau}$ vanish on Γ_N and on the Γ_D we can set $\phi = f$ due to (3.5). Overall we have

$$\int_{\Omega} (\sigma^{-1}\boldsymbol{j}\cdot\boldsymbol{\tau} - \phi\,\mathrm{div}\,\boldsymbol{\tau})\,\mathrm{d}x + \int_{\Gamma_D} f\boldsymbol{\tau}\cdot\boldsymbol{n}\,\mathrm{d}S + \int_{\Gamma_{\mathrm{MO}}(t)} [[\phi]]\boldsymbol{\tau}\cdot\boldsymbol{n}_{\Gamma_{\mathrm{MO}}}\,\mathrm{d}S = 0. \tag{3.14}$$

Plugging (3.9) into previous equality finishes this derivation. We have rewritten our problem into equations (3.13) and (3.14). This gives *a clue* about a weak formulation. More legitimate definition is given in the following subsection.

Back to the jump at OE interface. Adding Ω_e into the formulation is simple and the only difference is in additional interfacial integral. The equation (3.13) has integration over Ω_e also and (3.14) becomes

$$\int_{\Omega} (\sigma^{-1}\boldsymbol{j}\cdot\boldsymbol{\tau} - \phi\,\mathrm{div}\,\boldsymbol{\tau})\,\mathrm{d}x + \int_{\Gamma_D} f\boldsymbol{\tau}\cdot\boldsymbol{n}\,\mathrm{d}S + \int_{\Gamma_{\mathrm{MO}}(t)} [[\phi]]\boldsymbol{\tau}\cdot\boldsymbol{n}_{\Gamma_{\mathrm{MO}}}\,\mathrm{d}S \tag{3.15}$$

$$+ \int_{\Gamma_{\mathrm{OE}}(t)} [[\phi]]\boldsymbol{\tau}\cdot\boldsymbol{n}_{\Gamma_{\mathrm{OE}}}\,\mathrm{d}S = 0. \tag{3.16}$$

3.2.3 Mixed weak formulation

Let Ω be domain defined in the previous section. The **mixed formulation** of our problem is to find $(\boldsymbol{j}, \phi) \in \boldsymbol{H}\times Q$, such that

$$a(\boldsymbol{j},\boldsymbol{\tau}) + b(\boldsymbol{\tau},\phi) = F(\boldsymbol{\tau}) \quad \forall\boldsymbol{\tau}\in\boldsymbol{H}, \tag{3.17}$$

$$b(\boldsymbol{j}, v) = 0 \quad \forall v \in Q. \tag{3.18}$$

The mappings $a(\cdot,\cdot) : \boldsymbol{H}\times\boldsymbol{H} \longrightarrow \mathbb{R}$ and $b(\cdot,\cdot) : \boldsymbol{H}\times Q \longrightarrow \mathbb{R}$ are defined as

$$a(\boldsymbol{j},\boldsymbol{\tau}) := \int_{\Omega} \sigma^{-1}\boldsymbol{j}\cdot\boldsymbol{\tau}\,\mathrm{d}x + \tag{3.19}$$

$$+ \langle g_{\mathrm{MO}}(\mathrm{Tr}_{\boldsymbol{n}_{\Gamma_{\mathrm{MO}}}}(\boldsymbol{j})), \mathrm{Tr}_{\boldsymbol{n}_{\Gamma_{\mathrm{MO}}}}(\boldsymbol{\tau})\rangle_{\Gamma_{\mathrm{MO}}} + \tag{3.20}$$

$$+ \langle g_{\mathrm{OE}}(\mathrm{Tr}_{\boldsymbol{n}_{\Gamma_{\mathrm{OE}}}}(\boldsymbol{j})), \mathrm{Tr}_{\boldsymbol{n}_{\Gamma_{\mathrm{OE}}}}(\boldsymbol{\tau})\rangle_{\Gamma_{\mathrm{OE}}}, \tag{3.21}$$

$$b(\boldsymbol{\tau},\phi) := -\int_{\Omega} \phi\,\mathrm{div}\,\boldsymbol{\tau}\,\mathrm{d}x\,, \tag{3.22}$$

with $g_{\mathrm{MO}} : \mathrm{H}^{-1/2}(\Gamma_{\mathrm{MO}}) \longrightarrow \mathrm{H}^{1/2}(\Gamma_{\mathrm{MO}}), g_{\mathrm{OE}} : \mathrm{H}^{-1/2}(\Gamma_{\mathrm{OE}}) \longrightarrow \mathrm{H}^{1/2}(\Gamma_{\mathrm{OE}})$ and $+\infty > \sup_{\boldsymbol{x}\in\Omega}\sigma(\boldsymbol{x}) \geq \sigma(\boldsymbol{x}) \geq \inf_{\boldsymbol{x}\in\Omega}\sigma(\boldsymbol{x}) > 0$ being bounded from above and from below. The operator $\mathrm{Tr}_{\boldsymbol{n}}$ is the normal trace operator from Theorem 1 in Appendix A.

Function spaces are denoted

$$\boldsymbol{H} := \mathrm{H}(\mathrm{div}, \Omega) = \{\boldsymbol{\tau} \in (\mathrm{L}^2(\Omega))^d;\ \mathrm{div}\,\boldsymbol{\tau} \in \mathrm{L}^2(\Omega) \text{ in the distributional sense}, \\ \mathrm{Tr}_{\boldsymbol{n}_{\Gamma_N}}(\boldsymbol{\tau}) = 0\},$$

$$Q := \mathrm{L}^2(\Omega).$$

The non-trivial aspect of this problem is the second and third term in the mapping $a(\cdot,\cdot)$. The structure of this functional motivates us to write

$$a(\boldsymbol{j}, \boldsymbol{\tau}) := a_1(\boldsymbol{j}, \boldsymbol{\tau}) + a_2(\boldsymbol{j}, \boldsymbol{\tau}),$$

$$a_1(\boldsymbol{j}, \boldsymbol{\tau}) := \int_\Omega \sigma^{-1} \boldsymbol{j} \cdot \boldsymbol{\tau}\, \mathrm{d}x\,, \tag{3.23}$$

$$a_2(\boldsymbol{j}, \boldsymbol{\tau}) := \langle g_{\mathrm{MO}}(\mathrm{Tr}_{\boldsymbol{n}_{\Gamma_{\mathrm{MO}}}}(\boldsymbol{j})), \mathrm{Tr}_{\boldsymbol{n}_{\Gamma_{\mathrm{MO}}}}(\boldsymbol{\tau})\rangle_{\Gamma_{\mathrm{MO}}} + \\ + \langle g_{\mathrm{OE}}(\mathrm{Tr}_{\boldsymbol{n}_{\Gamma_{\mathrm{OE}}}}(\boldsymbol{j})), \mathrm{Tr}_{\boldsymbol{n}_{\Gamma_{\mathrm{OE}}}}(\boldsymbol{\tau})\rangle_{\Gamma_{\mathrm{OE}}} \tag{3.24}$$

and we will refer to the a_2 as to the **jump functional**, since it reproduces the conditions (3.9), (3.10). Clearly, the a_1 is bounded and linear while properties of a_2 depends on non-linearities in $g_{\mathrm{MO}}(\cdot)$ and $g_{\mathrm{OE}}(\cdot)$.

On the right hand side there is a functional $F \in \boldsymbol{H}^*$ defined as

$$F(\boldsymbol{\tau}) := -\langle f, \mathrm{Tr}_{\boldsymbol{n}_{\Gamma_D}}(\boldsymbol{\tau})\rangle_{\Gamma_D}, \tag{3.25}$$

for $f \in \mathrm{H}^{1/2}(\Gamma_D)$. The continuity and boundedness of the normal trace operator, $\mathrm{Tr}_{\boldsymbol{n}}$, assures that F is indeed in the dual space to $\boldsymbol{H}$.

3.2.4 Existence and uniqueness

Let us now prove the existence of solution to the problem (3.17), (3.18). The proof is based on little adjustment of standard mixed Stokes problem proof, see [Süli, 2013]. In the standard mixed proof all of the functionals are linear, while here the jump functional a_2 is not. This is dealt with the use of (generalized) non-linear version of Lax-Milgram lemma, see Appendix A Theorem 3 [3], instead of its linear counterpart.

Let us define the closed linear subspace $\boldsymbol{V} \subset \boldsymbol{H}$ where functional b vanishes, i.e.

$$\boldsymbol{V} := \{\boldsymbol{v} \in \boldsymbol{H};\ b(\boldsymbol{v}, q) = 0 \quad \forall q \in Q\}. \tag{3.26}$$

In other words, the space $\boldsymbol{V}$ is a space of divergence-free functions. Choosing a test function $\boldsymbol{\tau} \in \boldsymbol{V} \subset \boldsymbol{H}$ we have from (3.18) and (3.17) simply

$$a(\boldsymbol{j}, \boldsymbol{\tau}) = F(\boldsymbol{\tau}), \qquad \forall \boldsymbol{\tau} \in \boldsymbol{V}. \tag{3.27}$$

Because $\boldsymbol{V}$ is a Hilbert space equipped with scalar product and norm from the space $\boldsymbol{H}$ we have trivial isometric embedding of $\boldsymbol{V}$ into $\boldsymbol{H}$.

By the non-linear Lax-Milgram we have the existence of unique $\boldsymbol{j}_0 \in \boldsymbol{V}$ fulfilling (3.27). This function $\boldsymbol{j}_0$ automatically satisfies (3.18). In more detail, the

[3] In some literature this is called just Fixed point technique - since the proof of this lemma is based on straight use of Banach fixed point theorem.

non-linear Lax-Milgram lemma requires a to be **strongly monotone**, see Appendix A, Definition 1, and **Lipschitz continuous**, see Appendix A, Definition 2. The functional a has an inner structure, so we need to examine it further.

Lipschitz continuity for a_1 is trivial, since

$$\left|\int_\Omega \sigma^{-1}(\boldsymbol{j}_1-\boldsymbol{j}_2)\cdot\boldsymbol{\tau}\,\mathrm{d}x\right| \leq \frac{1}{\inf\sigma}\int_\Omega |(\boldsymbol{j}_1-\boldsymbol{j}_2)\cdot\boldsymbol{\tau}|\,\mathrm{d}x \leq \frac{1}{\inf\sigma}\|\boldsymbol{j}_1-\boldsymbol{j}_2\|_{\mathrm{L}^2}\|\boldsymbol{\tau}\|_{\mathrm{L}^2} = \\ = \frac{1}{\inf\sigma}\|\boldsymbol{j}_1-\boldsymbol{j}_2\|_{\boldsymbol{V}}\|\boldsymbol{\tau}\|_{\boldsymbol{V}}.$$

The last equality is important and follows from the fact, that space $\boldsymbol{V}$ is a space of divergence free functions.

In order to satisfy the Lipschitz continuity of a_2 we have to assume, that $g_{\mathrm{MO}}:\mathrm{H}^{-1/2}(\Gamma_{\mathrm{MO}})\longrightarrow\mathrm{H}^{1/2}(\Gamma_{\mathrm{MO}})$ and $g_{\mathrm{OE}}:\mathrm{H}^{-1/2}(\Gamma_{\mathrm{MO}})\longrightarrow\mathrm{H}^{1/2}(\Gamma_{\mathrm{MO}})$ are **Lipschitz continuous**. Then (for MO interface, since OE is treated in the same way)

$$\begin{aligned}
&\left|\langle g_{\mathrm{MO}}(\mathrm{Tr}_{\boldsymbol{n}_{\Gamma_{\mathrm{MO}}}}(\boldsymbol{j}_1)) - g_{\mathrm{MO}}(\mathrm{Tr}_{\boldsymbol{n}_{\Gamma_{\mathrm{MO}}}}(\boldsymbol{j}_2)), \mathrm{Tr}_{\boldsymbol{n}_{\Gamma_{\mathrm{MO}}}}(\boldsymbol{\tau})\rangle_{\Gamma_{\mathrm{MO}}}\right| \leq \\
&\leq \left\|g_{\mathrm{MO}}(\mathrm{Tr}_{\boldsymbol{n}_{\Gamma_{\mathrm{MO}}}}(\boldsymbol{j}_1)) - g_{\mathrm{MO}}(\mathrm{Tr}_{\boldsymbol{n}_{\Gamma_{\mathrm{MO}}}}(\boldsymbol{j}_2))\right\|_{\mathrm{H}^{1/2}(\Gamma_{\mathrm{MO}})}\left\|\mathrm{Tr}_{\boldsymbol{n}_{\Gamma_{\mathrm{MO}}}}(\boldsymbol{\tau})\right\|_{\mathrm{H}^{-1/2}(\Gamma_{\mathrm{MO}})} \leq \\
&\leq L\left\|\mathrm{Tr}_{\boldsymbol{n}_{\Gamma_{\mathrm{MO}}}}(\boldsymbol{j}_1) - \mathrm{Tr}_{\boldsymbol{n}_{\Gamma_{\mathrm{MO}}}}(\boldsymbol{j}_2)\right\|_{\mathrm{H}^{-1/2}(\Gamma_{\mathrm{MO}})}\left\|\mathrm{Tr}_{\boldsymbol{n}_{\Gamma_{\mathrm{MO}}}}(\boldsymbol{\tau})\right\|_{\mathrm{H}^{-1/2}(\Gamma_{\mathrm{MO}})} \leq \\
&\leq LC^{\mathrm{Tr}}\|\boldsymbol{j}_1-\boldsymbol{j}_2\|_{\boldsymbol{V}}\|\boldsymbol{\tau}\|_{\boldsymbol{V}}
\end{aligned}$$

due to the normal trace theorem and again, vanishing divergence of functions from $\boldsymbol{V}$. Because both, a_1 and a_2 are Lipschitz continuous so is their sum, a.

Strong monotone property of a_1 is also simple,

$$\int_\Omega \sigma^{-1}(\boldsymbol{j}_1-\boldsymbol{j}_2)\cdot(\boldsymbol{j}_1-\boldsymbol{j}_2)\,\mathrm{d}x \geq \frac{1}{\sup\sigma}\|\boldsymbol{j}_1-\boldsymbol{j}_2\|^2_{\boldsymbol{V}}.$$

Strong monotone property of a_2 (and of $g_{\mathrm{MO/OE}}$ in consequence) could be assumed, but it is not necessary. We need only $g_{\mathrm{MO/OE}}$ be **monotone**. Then the whole functional is strongly monotone, i.e.

$$\int_\Omega \sigma^{-1}(\boldsymbol{j}_1-\boldsymbol{j}_2)\cdot(\boldsymbol{j}_1-\boldsymbol{j}_2)\,\mathrm{d}x + \langle g(\mathrm{Tr}_{\boldsymbol{n}_{\Gamma_I}}(\boldsymbol{j}_1)) - g(\mathrm{Tr}_{\boldsymbol{n}_{\Gamma_I}}(\boldsymbol{j}_2)), \mathrm{Tr}_{\boldsymbol{n}_{\Gamma_{\mathrm{MO}}}}(\boldsymbol{j}_1-\boldsymbol{j}_2)\rangle_{\Gamma_{\mathrm{MO}}} \geq \\
\geq \int_\Omega \sigma^{-1}(\boldsymbol{j}_1-\boldsymbol{j}_2)\cdot(\boldsymbol{j}_1-\boldsymbol{j}_2)\,\mathrm{d}x \geq \frac{1}{\sup\sigma}\|\boldsymbol{j}_1-\boldsymbol{j}_2\|^2_{\boldsymbol{V}}.$$

In summary, assumptions of non-linear Lax-Milgram lemma are satisfied for $g_{\mathrm{MO/OE}}$ being Lipschitz continuous and monotone.

Now, we need to show the existence of unique ϕ_0 such that (3.17) holds. For the found and fixed $\boldsymbol{j}_0$ we are looking for ϕ_0 fulfilling $b(\boldsymbol{\tau},\phi_0) = F(\boldsymbol{\tau}) - a(\boldsymbol{j}_0,\boldsymbol{\tau})$ for all $\boldsymbol{\tau}\in\boldsymbol{H}$. Recall that $b(\cdot,\cdot)$ is a bounded bilinear functional on $\boldsymbol{H}\times Q$ and the right hand side mapping $\mathcal{L}:\boldsymbol{\tau}\mapsto F(\boldsymbol{\tau}) - a(\boldsymbol{j}_0,\boldsymbol{\tau})$ is a linear and bounded

mapping from $\boldsymbol{H}$ to real numbers. In other words, our sub-problem could be rewritten: find $\phi_0 \in Q$ such that

$$b(\boldsymbol{\tau}, \phi_0) = \mathcal{L}(\boldsymbol{\tau}) \quad \forall \boldsymbol{\tau} \in \boldsymbol{H}. \tag{3.28}$$

For these type of problems, where bilinear functional maps cartesian product of two different Hilbert spaces, so called inf-sup condition on b must be fulfilled. Fortunately, the functional b in our paper is a standard functional from mixed Stokes problem and the validity of inf-sup condition could be found in most of books on this topic, [Boffi et al., 2013], [Gatica, 2014]. Our only difference, the non-linear jump functional doesn't play any role here, since $\boldsymbol{j}_0$ is fixed and hidden inside $\mathcal{L}$.

Referring to the standard results we have the existence and uniqueness of $\phi_0 \in Q$ satisfying (3.28).

Summing up, we have shown the existence and uniqueness of $\boldsymbol{j}_0 \in \boldsymbol{H}$ satisfying (3.27) and existence and uniqueness of $\phi_0 \in Q$ satisfying (3.28). This piece-wise strategy is put together and the couple $(\boldsymbol{j}_0, \phi_0)$ is the desired solution.

3.3 Interface evolution

The problem of nanoporous structure evolution is a problem with evolving free boundary. The basic physical mechanism which evolves the boundaries (interfaces) is metal oxidation, summarized in Section 2.6, point ②. By the nature of oxidation reaction the interfaces are not *material surfaces*, i.e. they are not composed of the same physical species (molecules, atoms) at every time. This determines the actual mathematical equation which is used to solve boundary movement.

Let us think, that we are given scalar quantitity, $c_o : [0, T] \times \Omega \longrightarrow \mathbb{R}$, which describes a "concentration" of oxide. [4] Advection-reaction equation (or one can say: continuity equation with sources/sinks) for this quantity reads

$$\frac{\partial c_o}{\partial t} + \operatorname{div}(\boldsymbol{u} c_o) = r_{\mathrm{MO}} + r_{\mathrm{OE}},$$

without giving it precise mathematical meaning for now.

The first term represents change in oxide concentration, the second term is responsible for advection in external velocity field $\boldsymbol{u}$ and the term on right hand side is called reaction-rate term. It usually comes from chemical reactions occuring inside Ω.

If we assume there are no advective fluxes ($\boldsymbol{u} = 0$) and the only change in concentration is due to source/sink right hand side term we have

$$\frac{\partial c_o}{\partial t} = r_{\mathrm{MO}} + r_{\mathrm{OE}}.$$

Reaction rates could be present in whole domain Ω, on some $k < d, k \in \mathbb{N}$ dimensional interfaces [5] or even at a single point. In this work $k = d - 1$ and

[4] This quantity will be formalised in the following section about level-set method. Unlike in *phase-field* methods, it doesn't describe real physical concentration of the oxide phase. It is purely mathematical construction to tell if we are inside of the oxide or not.

[5] By the dimension of the interface we mean it's topological dimension, i.e. dimension of the interface as a smooth manifold.

usually we have $d = 2$. This type of coupling is in literature often called 2d-1d coupling. Vaguely speaking, we are interested in reactions occuring at MO and OE interfaces so we can write

$$\frac{\partial c_o}{\partial t} = r_{\mathrm{MO}}\delta_{\Gamma_{\mathrm{MO}}} + r_{\mathrm{OE}}\delta_{\Gamma_{\mathrm{OE}}}$$

for the evolution of oxide layer due to OE and MO interfatial reactions. The $\delta_{\Gamma_{\mathrm{OE}}}$ is dirac delta measure concentrated at OE interface, similarly for the MO interface. Reaction rates $r_{\mathrm{MO}}, r_{\mathrm{OE}}$ are functions of normal component of electric current given by the right hand sides in (2.19) and (2.18).

Mathematically more pleasing formulation will be clear in the following subsection.

3.3.1 Weak formulation

We will formulate this problem after we perform finite difference discretization in time. This approach is more similar to the way we actually solve the equations. Additionally, fully coupled time problem would be very challenging, since subdomains (and their regularity) change in time.

The discrete-in-time problem reads: for a given time step k, given previous time step solution $c^k \in S$, given total current density $\boldsymbol{j}^k \in \mathrm{H}(\mathrm{div}, \Omega)$ find $c^{k+1} \in S$ such that

$$\left(\frac{c^{k+1} - c^k}{\Delta t}, v\right)_{\mathrm{L}^2(\Omega)} = \langle r_{\mathrm{MO}}(\boldsymbol{j}^k \cdot \boldsymbol{n}), v\rangle_{\Gamma_{\mathrm{MO}}} + \langle r_{\mathrm{OE}}(\boldsymbol{j}^k \cdot \boldsymbol{n}), v\rangle_{\Gamma_{\mathrm{OE}}} \quad \forall v \in S, \tag{3.29}$$

with

$$S := \{s \in \mathrm{H}^1(\Omega); s = 0 \text{ on } \Gamma_D \text{ in the sense of trace}\}$$

and $r_{\mathrm{MO}} : \mathbb{R} \longrightarrow \mathbb{R}, r_{\mathrm{OE}} : \mathbb{R} \longrightarrow \mathbb{R}$ are defined as

$$r_{\mathrm{MO}}(x) := x t_O \frac{M_{\mathrm{TiO_2}}}{4\rho_{\mathrm{TiO_2}} F},$$
$$r_{\mathrm{OE}}(x) := x(t_O - \varepsilon^k)\frac{M_{\mathrm{TiO_2}}}{4\rho_{\mathrm{TiO_2}} F}.$$

We must be careful with duality pairing (between $\mathrm{H}^{-1/2}$ and $\mathrm{H}^{1/2}$) in (3.29). Because r_{MO} is linear (with respect to $\boldsymbol{j}^k$) we could define their action on a $\mathrm{H}^{-1/2}$ distribution due to the normal trace theorem (Green's identity for $\mathrm{H}(\mathrm{div}, \Omega)$, see Theorem 2 in Appendix A), i.e.

$$\langle r_{\mathrm{MO}}(\boldsymbol{j}^k \cdot \boldsymbol{n}), v\rangle_{\Gamma_{\mathrm{MO}}} := \int_{\Omega_o} r_{\mathrm{MO}}(\mathrm{div}\, \boldsymbol{j}^k) v \,\mathrm{d}x + \int_{\Omega_o} r_{\mathrm{MO}}(\boldsymbol{j}^k) \cdot \mathrm{grad}\, v \,\mathrm{d}x\,.$$

More problematic is the term r_{OE}. Due to the current efficiency ε, this term is highly non-linear. It is not possible to define non-linear mapping of a $\mathrm{H}^{-1/2}$ distribution. In order to $\varepsilon(\boldsymbol{j}^k \cdot \boldsymbol{n})$ make sense we must assume that $\boldsymbol{j}^k \cdot \boldsymbol{n} \in \mathrm{L}^2(\Gamma_{\mathrm{OE}})$.

4. Numerical model

In this chapter, infinite-dimensional equations formulated above are discretized. We are interested in a numerical solution to the problems: high-field conduction law, continuity equation with jumps and inteface evolution. Each of the problem is addressed in an individual section.

Generally speaking, spatial discretization is always treated with the use of *finite element method*, while temporal discretization is dealt with a *finite difference scheme*.

4.1 Characteristic level-set method

Motivation for the use of a level-set method is straightforward. Interfaces MO and OE must be tracked and evolved in time. The aim is also to approximate interfacial integrals over $\Gamma_{\mathrm{MO}}, \Gamma_{\mathrm{OE}}$ in (3.21).

One could use methods where interface is approximated with edges of triangles (or faces of tetrahedra) - so called conforming mesh would need to be constructed. This is a common approach in finite element method.

Another technique is based on so called characteristic level-set function. We say, that $\varphi_\varepsilon \in \mathrm{C}^\infty(\overline{\Omega}, \mathbb{R})$ is a **characteristic level-set function of an interface** Γ, iff

$$\Gamma := \{\boldsymbol{x} \in \Omega; \varphi_\varepsilon(\boldsymbol{x}) = K\}, \tag{4.1}$$

$$\int_\Omega |\mathrm{grad}\, \varphi_\varepsilon| f \,\mathrm{d}x \longrightarrow \int_\Gamma f \,\mathrm{d}S\,, \quad \text{as } \varepsilon \longrightarrow 0^+, \forall f \in \mathrm{H}^1(\Omega) \tag{4.2}$$

for a given $K \in \mathbb{R}$. The property (4.1) is the standard level-set property. It tells which "slice" of the function φ_ε represents the interface. The property (4.2) is connected with the adjective *characteristic* in the name of the method. This function approximates the characteristic function of a domain, which boundary is the interface Γ.

An example of such function with its derivative in one dimension is

$$\varphi_\varepsilon := \frac{1}{1 + \mathrm{e}^{x/\varepsilon}}, \quad |\mathrm{grad}\, \varphi_\varepsilon| = \frac{(\varphi_\varepsilon)^2}{\varepsilon} \mathrm{e}^{x/\varepsilon}. \tag{4.3}$$

It is shown in Figure 4.1.

So far, only one characteristic funtion was discussed, called φ_ε. Our interest is in approximation of two interfaces and we need two characteristic level-set functions. Let us call a function describing the MO interface $\varphi_{\varepsilon,\mathrm{MO}}$ and a function describing the OE interface $\varphi_{\varepsilon,\mathrm{OE}}$. [1] One-dimensional illustration of these functions is in Figure 4.2. Note, that function $\varphi_{\varepsilon,\mathrm{OE}}$ is not a smoothed characteristic function of the oxide phase but of metal+oxide phase together. This way we can represent characteristic function of the oxide phase as $\varphi_{\varepsilon,\mathrm{OE}} - \varphi_{\varepsilon,\mathrm{MO}}$.

With the use of the property (4.2) we can approximate the jump functional a_2 (3.24). More precisely, for $\boldsymbol{j}, \boldsymbol{\tau} \in (\mathrm{H}^1(\Omega))^d$ the duality on $\Gamma_{\mathrm{MO/OE}}$ is represented

[1] We sometimes drop the ε subindex for brevity.

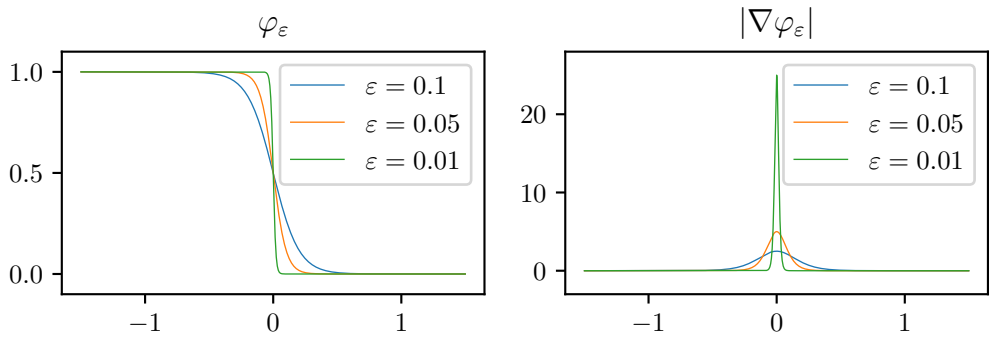

Figure 4.1: An example of a one-dimensional level-set function.
It is clearly visible how $\varepsilon \longrightarrow 0$ approximates the characteristic function of $(-\infty, 0)$.

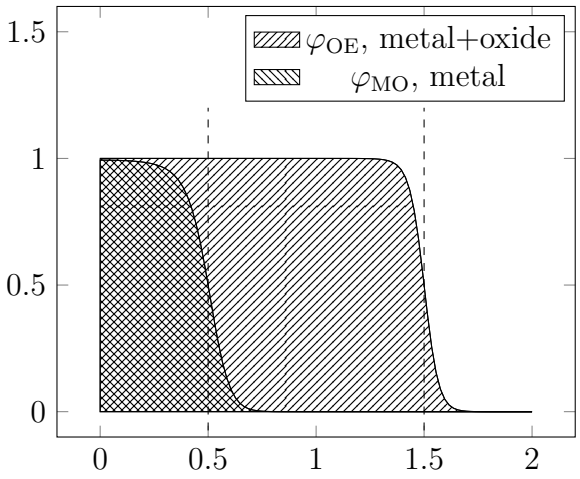

Figure 4.2: One-dimensional illustration of two (characteristic) level-set functions.
The interfaces are shown as the dashed vertical lines.

via L^2 scalar product (Theorem 1 in Appendix A), so we have

$$a_2(\boldsymbol{j}, \boldsymbol{\tau}) = \int_{\Gamma_{\mathrm{MO}}} g_{\mathrm{MO}}(\boldsymbol{j} \cdot \boldsymbol{n}_{\Gamma_{\mathrm{MO}}}) \boldsymbol{\tau} \cdot \boldsymbol{n}_{\Gamma_{\mathrm{MO}}} \,\mathrm{d}S + \int_{\Gamma_{\mathrm{OE}}} g_{\mathrm{OE}}(\boldsymbol{j} \cdot \boldsymbol{n}_{\Gamma_{\mathrm{OE}}}) \boldsymbol{\tau} \cdot \boldsymbol{n}_{\Gamma_{\mathrm{OE}}} \,\mathrm{d}S$$

and using the definitions of normal vectors, i.e.

$$\boldsymbol{n}_{\Gamma_{\mathrm{MO}}} := \frac{-\operatorname{grad} \varphi_{\varepsilon,\mathrm{MO}}}{|\operatorname{grad} \varphi_{\varepsilon,\mathrm{MO}}|},$$
$$\boldsymbol{n}_{\Gamma_{\mathrm{OE}}} := \frac{-\operatorname{grad} \varphi_{\varepsilon,\mathrm{OE}}}{|\operatorname{grad} \varphi_{\varepsilon,\mathrm{OE}}|}$$

and (4.2) one arrives at

$$a_{2,\varepsilon}(\boldsymbol{j},\boldsymbol{\tau}) := \int_\Omega g_{\mathrm{MO}}\left(\boldsymbol{j}\cdot\frac{-\operatorname{grad}\varphi_{\varepsilon,\mathrm{MO}}}{|\operatorname{grad}\varphi_{\varepsilon,\mathrm{MO}}|}\right)(\boldsymbol{\tau}\cdot\operatorname{grad}\varphi_{\varepsilon,\mathrm{MO}})\,\mathrm{d}x + \\ + \int_\Omega g_{\mathrm{OE}}\left(\boldsymbol{j}\cdot\frac{-\operatorname{grad}\varphi_{\varepsilon,\mathrm{OE}}}{|\operatorname{grad}\varphi_{\varepsilon,\mathrm{OE}}|}\right)(\boldsymbol{\tau}\cdot\operatorname{grad}\varphi_{\varepsilon,\mathrm{OE}})\,\mathrm{d}x\,,$$

with

$$a_{2,\varepsilon}(\boldsymbol{j},\boldsymbol{\tau}) \longrightarrow a_2(\boldsymbol{j},\boldsymbol{\tau}).$$

The level-set function isn't used solely to approximate the jump functional a_2. The function (conductivity) σ is approximated also as

$$\sigma_\varepsilon := \sigma_m^{\varphi_{\varepsilon,\mathrm{MO}}}\sigma_o^{(1-\varphi_{\varepsilon,\mathrm{MO}})\varphi_{\varepsilon,\mathrm{OE}}}\sigma_e^{(1-\varphi_{\varepsilon,\mathrm{MO}})(1-\varphi_{\varepsilon,\mathrm{OE}})}.$$

With the aid of the approximated conductivity we can write approximation to functional a_1. Indeed

$$a_{1,\varepsilon}(\boldsymbol{j},\boldsymbol{\tau}) := \int_\Omega \sigma_\varepsilon^{-1}\boldsymbol{j}\cdot\boldsymbol{\tau}\,\mathrm{d}x\,.$$

The level-set approximate problem for mixed formulation is the same as in (3.17), (3.18), but taking an approximation to a as

$$a_\varepsilon := a_{1,\varepsilon} + a_{2,\varepsilon}. \tag{4.4}$$

The problem of interface evolution also contains dualities on the MO/OE interfaces. We can utilize the level-set method to approximate these also. Thanks to the property (4.2) dualities in (3.29) are approximated in a similar fashion as above, i.e.

$$\langle r_{\mathrm{MO/OE}}(\boldsymbol{j}^k\cdot\boldsymbol{n}), v\rangle_{\Gamma_{\mathrm{MO/OE}}} \approx \int_\Omega r_{\mathrm{MO/OE}}\left(\boldsymbol{j}^k\cdot\frac{-\operatorname{grad}\varphi_{\varepsilon,\mathrm{MO/OE}}}{\left|\operatorname{grad}\varphi_{\varepsilon,\mathrm{MO/OE}}\right|}\right)v\left|\operatorname{grad}\varphi_{\varepsilon,\mathrm{MO/OE}}\right|\,\mathrm{d}x\,. \tag{4.5}$$

This (characteristic level-set) formulation has several advantages over the methods mentioned before. The most functional aspect is the implicit description of interface $\Gamma_{\mathrm{MO}}, \Gamma_{\mathrm{OE}}$. Because the geometry changes and $\Omega_m = \Omega_m(t), \Omega_o = \Omega_o(t), \Omega_e = \Omega_e(t)$ are time-dependent domains, level-set function is evolved accordingly.

4.2 Finite element discretization

Spatial partial differential equations in this thesis are discretized with the use of the *finite element method*, see [Brenner and Scott, 2007].

We restrict ourself to cases where dimension $d = 2$. Let Ω be the same as in the previous section, let moreover Γ be its polygonal or polyhedral boundary and $\mathcal{T}_h$ a finite triangularization of $\overline{\Omega}$, i.e. $\overline{\Omega} = \bigcup_{r=1}^{m}\overline{K_r}, K_r \in \mathcal{T}_h$.

We call K_r an element. In this thesis we use simplicial elements, in $d = 2$ triangles. The edges are denoted $e_i, i \in \{1, 2, 3\}$. The index h is, as usual, the minimum diameter of the elements of the decomposition. This index is sometimes refered also as a discretization parameter. In the following sections, functions with subindex h denote a Galerkin approximation to functions without the subindex. For example, ϕ_h is a finite-dimensional Galerkin finite element approximation to an abstract, infinite dimensional electrostatic potential ϕ.

Discretized equations are implemented in finite element library *FEniCS 2017.1* [Alnæs et al., 2015].

4.3 Finite elements for high-field conduction law

The basic (infinite-dimensional) problem is stated in section 3.1. In this section finite element approximation to the level-set function of the MO and OE interface on time level k is denoted just φ_{MO} and φ_{OE}.

Finite element formulation of this problem reads: find $\bar{\phi}_h \in V_h$ such that

$$\boxed{\left(\sigma(\bar{\phi}_h)\operatorname{grad}\bar{\phi}_h, \operatorname{grad} v_h\right)_{\mathrm{L}^2(\Omega)} = 0, \quad \forall v_h \in V_h} \tag{4.6}$$

with non-linear conductivity inside the oxide domain as

$$\sigma_o(\bar{\phi}_h) := \sum_{i\in\mathrm{ions}} C_i u_i^0 \frac{1}{\left|\operatorname{grad}\bar{\phi}_h\right|} \sinh\left(\frac{z_i a F\left|\operatorname{grad}\bar{\phi}_h\right|}{RT}\right)$$

and overall conductivity composed with the help of level-set function as

$$\sigma_\varepsilon := \sigma_m^{\varphi_{\mathrm{MO}}} \sigma_o^{(1-\varphi_{\mathrm{MO}})\varphi_{\mathrm{OE}}} \sigma_e^{(1-\varphi_{\mathrm{MO}})(1-\varphi_{\mathrm{OE}})}.$$

Finite element space used

$$V_h := \{v \in V, \forall K \in \mathcal{T}_h : v \in P_k(K)\}$$

where k is the degree of finite element functions used (the same for all K), i.e. P_k is the space of polynomials up to (and equal) degree k. We will refer to this finite element space usually as $\mathcal{CG}_k$ (continuous galerkin of degree k).

The function σ is a non-linear function of the finite element solution ϕ_h. We are using classical *Newton-Raphson method* to linearize and solve the equations. The system of linear equations is solved using `direct PETSc LU` solver.

4.4 Finite elements for mixed formulation for discontinuous solution

The basic (infinite-dimensional) problem is stated in subsection 3.2.3. Finite element formulation of this problem is a classical saddle-point problem: find $(\boldsymbol{j}_h, \phi_h) \in \boldsymbol{H}_h \times Q_h$ such that

$$\boxed{\begin{aligned} a_\varepsilon(\boldsymbol{j}_h, \boldsymbol{\tau}_h) + b(\boldsymbol{\tau}_h, \phi_h) &= F(\boldsymbol{\tau}_h) \quad \forall \boldsymbol{\tau}_h \in \boldsymbol{H}_h, \qquad (4.7)\\ b(\boldsymbol{j}_h, v_h) &= 0 \quad \forall v_h \in Q_h \qquad (4.8) \end{aligned}}$$

with a_ε defined in (4.4), b and F the same as in (3.22) and (3.25).

We define

$$R_k(\partial K) := \{\phi; \phi \in \mathrm{L}^2(\partial K); \phi|_{e_i} \in P_k(e_i), \forall e_i)\}$$

where P_k are polynomials of degree $\leq k$. It is a space of functions with polynomial traces on edges of K.

Let us define also

$$\begin{aligned} \boldsymbol{P}_k &:= (P_k(K))^d, \\ \boldsymbol{P}_k^{\boldsymbol{n},s} &:= \{\boldsymbol{p} \in \boldsymbol{P}_k(K); \boldsymbol{p} \cdot \boldsymbol{n} \in R_s(\partial K)\} \end{aligned}$$

as a vector valued polynomials and vector valued polynomials with polynomial normal traces.

If we take a special case of vector valued polynomials of degree $\leq k$ with polynomial normal traces of degree $\leq s$ we obtain so called $\mathcal{BDM}$ or Brezzi-Douglas-Marini space. Formally

$$\mathcal{BDM}_k(K) := \boldsymbol{P}_k^{\boldsymbol{n},k}(K).$$

We construct finite dimensional approximations according to [Boffi et al., 2013] and inspired with the more simple problem where the nonlinear jump functional $a_2 = 0$. Therefore

$$\begin{aligned} \boldsymbol{H}_h &:= \{\boldsymbol{\tau}; \boldsymbol{\tau} \in \boldsymbol{H}; \boldsymbol{\tau}|_K \in \mathcal{BDM}_k, \forall K \in \mathcal{T}_h\}, \\ Q_h &:= \{v; v \in Q; v|_K \in P^{k-1}, \forall K \in \mathcal{T}_h\}. \end{aligned}$$

In other words, the standard mixed formulation of Laplace equation($a_2 = 0$) is $\inf - \sup$ stable for this choice of spaces.

Another possibility which satisfies discrete $\inf - \sup$ condition is Raviart-Thomas space $\mathcal{RT}_k$ with discontinuous piecewise polynomials of order k or Brezzi-Douglas-Fortin-Marini space $\mathcal{BDFM}_k$ with discontinuous piecewise polynomials of order k. Comprehensive analysis is found in [Boffi et al., 2013].

4.5 Finite elements and finite differences for interface evolution

The basic (infinite-dimensional) problem is stated in section 3.3. The "concentration" c^k is here replaced with two characteristic level-set functions $\varphi_{\mathrm{MO}}, \varphi_{\mathrm{OE}}$. This means, that two equations, each per level-set function, must be solved.

Finite element formulation for the discrete-in-space and discrete-in-time problem reads: for a given time step k, given previous time step solution $\varphi_{\mathrm{MO/OE}}^k \in S_h$, given total current density $\boldsymbol{j}_h^k \in \boldsymbol{H}_h$ find $\varphi_{\mathrm{MO/OE}}^{k+1} \in S_h$ such that

$$\boxed{\frac{1}{\Delta t}\left(\varphi_{\mathrm{MO/OE}}^{k+1} - \varphi_{\mathrm{MO/OE}}^k, v_h\right)_{\mathrm{L}^2(\Omega)} = \left(r_{\mathrm{MO/OE}}(\boldsymbol{j}_h^k \cdot \operatorname{grad} \varphi_{\mathrm{MO/OE}}^k), v_h\right)_{\mathrm{L}^2(\Omega)}} \quad (4.9)$$

for all $v_h \in S_h$ with

$$S_h := \{v \in S, \forall K \in \mathcal{T}_h : v \in P_k(K)\}$$

4.5.1 Reinitialization

The solution of (4.9) introduces spurious numerical artefacts. The property of level-set functions (4.2) is getting lost and the functions are loosing it's "sharpness", i.e. their ε-transition region is being diffused.

In order to address this unwelcome behaviour so-called *reinitialization* of level-set functions was introduced in [Olsson et al., 2007], [Olsson and Kreiss, 2005]. It is basically just a sharpening procedure where the functions are focused back to the initial state with well-controlled transition thickness region.

Assume we are given diffused level-set function of the MO/OE interface on time-level k, denoted $\varphi^k_{\mathrm{MO/OE}}$. Reinitialization consists of solving sub-time problems, i.e. finding $(\varphi^k)^{j+1}_{\mathrm{MO/OE}} \in W_h$ such that

$$\boxed{\begin{aligned} \frac{1}{\Delta\tau}\left((\varphi^k_{\mathrm{MO/OE}})^{j+1} - (\varphi^k_{\mathrm{MO/OE}})^{j}, q_h\right)_{\mathrm{L}^2(\Omega)} - \\ - \left(\boldsymbol{n}_{\Gamma_{\mathrm{MO/OE}}}(\varphi^k_{\mathrm{MO/OE}})^{j+1}[1-(\varphi^k_{\mathrm{MO/OE}})^{j+1}], \operatorname{grad} q_h\right)_{\mathrm{L}^2(\Omega)} = \\ = -\varepsilon\left(\operatorname{grad}(\varphi^k_{\mathrm{MO/OE}})^{j+1}, \operatorname{grad} q_h\right)_{\mathrm{L}^2(\Omega)} \end{aligned}} \tag{4.10}$$

for all $q_h \in W_h$ with

$$W_h := \{v \in \mathrm{H}^1(\Omega), \forall K \in \mathcal{T}_h : v \in P_k(K)\}.$$

It is very important to note, that the normal vector $\boldsymbol{n}_{\Gamma_{\mathrm{MO/OE}}}$ is kept constant with respect to index j.

Reinitialization parameters are $\Delta\tau$, a sub-time finite-difference discretization parameter and ε which determines the steady-state diffusion thickness of the level-set. These parameters are determined by the minimal finite element mesh cell diameter, h as

$$\Delta\tau := \frac{1}{2}h, \quad \varepsilon := \beta h.$$

The parameter β is usually set to 1. It linearly scales the level-set thickness with respect to the minimal cell diameter.

Illustration of the reinitialization effect on a diffused function is shown in Figure 4.3.

Reinitialization would never stop for $j \longrightarrow \infty$. We have to terminate the sub-time iteration for some $j = j_{\max}$. This $j_{\max}$ is determined with so called *steady-state* criterium. We define the steady-state with the help of functional

$$\begin{aligned} R^j(f_h, q_h) := \frac{1}{\Delta\tau}\left(f_h - (\varphi^k_{\mathrm{MO}})^j, q_h\right)_{\mathrm{L}^2(\Omega)} - \left(\boldsymbol{n}_{\Gamma_{\mathrm{MO}}} f_h(1-f_h), \operatorname{grad} q_h\right)_{\mathrm{L}^2(\Omega)} - \\ - \varepsilon\left(\operatorname{grad} f_h, \operatorname{grad} q_h\right)_{\mathrm{L}^2(\Omega)}. \end{aligned}$$

It is just rearranged formulation (4.10). Evaluating the functional R on each basis function of the space W_h (in both of its arguments) gives a matrix R_{mn}. We say, that $j = j_{\max}$ if

$$\left\|R^j_{mn}\right\|_\infty < \varepsilon_{\mathrm{reinit}}. \tag{4.11}$$

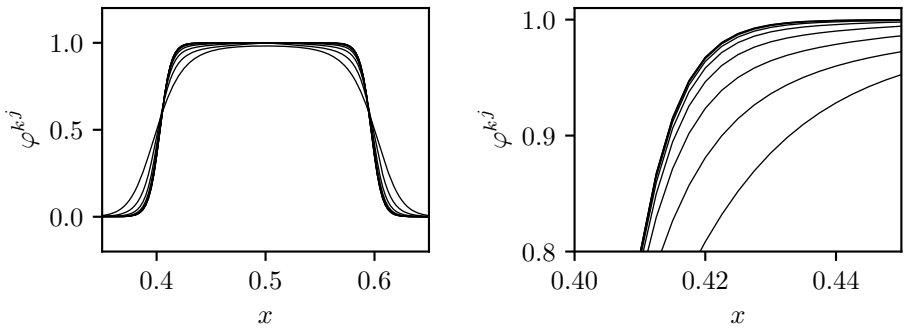

Figure 4.3: Focusing effect of the reinitialization.
One-dimensional initially diffused function is being focused to ε thickness. Several sub-time steps j are shown with solid lines. Approaching the steady state is clearly visible.

Parameter $\varepsilon_{\text{reinit}}$ is usually set to 10^{-5} if not specified otherwise.

We will conclude this section with a nice application of reinitialization to the advection equation. Consider one-dimensional example where characteristic function of some interval is advected in constant velocity field. Solving the advection equation (details are not important here, we want just to demonstrate the reinitialization effect) gives profiles for several times as in Figure 4.4.

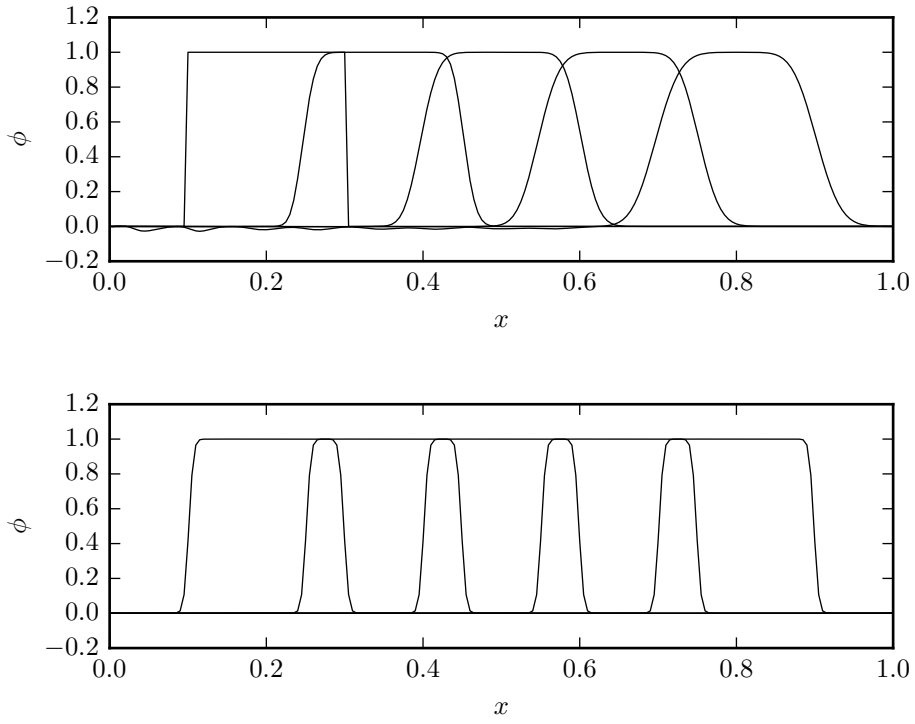

Figure 4.4: Advection of a characteristic function without (top) and with (bottom) reinitialization.

Notice how reinitialization maintains the thickness of the transition region of the characteristic function.

4.6 Overall solution strategy

Figure on the overall numerical picture is given in 4.5.

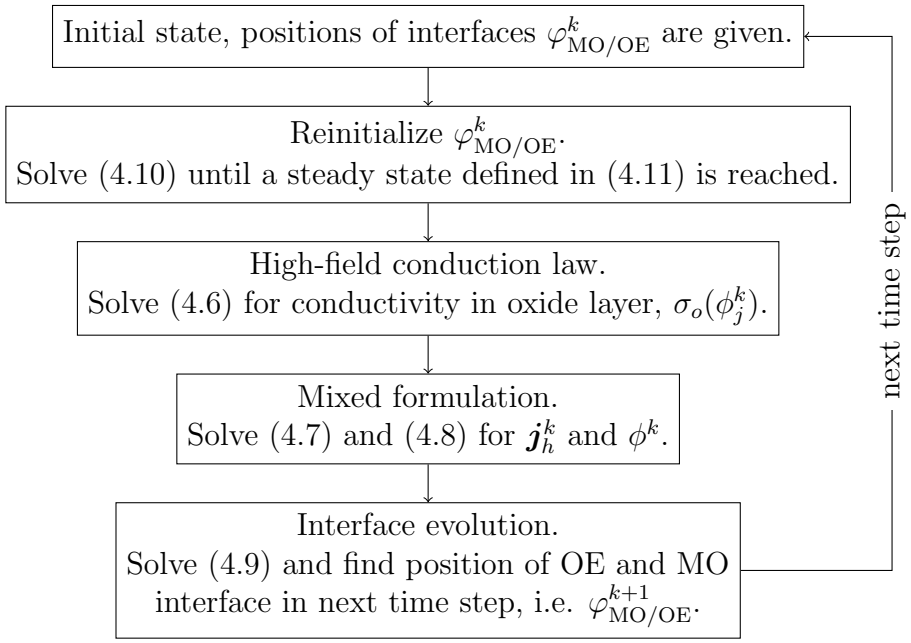

Figure 4.5: Overall numerical scheme.

5. Numerical tests

In the previous chapter several sub-problems were studied. We formulated high-field conduction law, mixed formulation for a solution with jumps and interface evolution with reinitialization.

Mixed formulation with electrochemically motivated non-linear jumps is the most novel contribution. For this reason we devote a big part of this chapter to the study of convergence of this formulation.

Later, we are able to connect each sub-problem into the overall model for the oxide growth.

5.1 Mixed formulation for discontinuous solution

Several numerical tests should be carried out for the level-set discrete problem (4.7) and (4.8). The aim of this section is to study the mixed formulation regardless of it's application in electrochemistry. We will find a potential with prescribed jump at an implicitly given interface.

Finite element mesh for one-dimensional examples is just a uniform partitioning of interval $(0, 1)$.

5.1.1 One dimension

Constant jump in one dimension

Consider a one-dimensional case $\Omega = (0, 1), \Gamma_D = \{0, 1\}, \Gamma_N = \emptyset$ where $g(\cdot) = g_0 \in \mathbb{R}$ is a constant function and there is only one interface, $\Gamma_I = \{0.5\}$.

Dimensionless boundary conditions and data are set to

$$\phi(0) = 1, \quad \phi(1) = 0, \quad \sigma_1 = 10, \quad \sigma_2 = 1 \tag{5.1}$$

with σ_1 and σ_2 being "conductivities" in the subdomains of Ω.

The sharp-interface (zero thickness of transition region, or in our case $\varepsilon = 0$) classical solution in one dimension with constant jump could be easily found. Indeed, one can check that the exact solution for the problem in subsection 3.2.1 is

$$\phi(x) = \begin{cases} \frac{2}{11}(g_0 - 1)x + 1, & \text{for} \quad x \in [0, 1/2), \\ \frac{20}{11}(g_0 - 1)(x - 1), & \text{for} \quad x \in (1/2, 1], \end{cases}$$

where g_0 is the discontinuity and the function $j = -\sigma \frac{\mathrm{d}\phi}{\mathrm{d}x}$ is constant for all $x \in (0, 1)$

$$j(x) = \frac{20}{11}(g_0 - 1).$$

These exact solutions will be used as a referential solution for error computation.

For the level-set discrete problem we choose a characteristic level-set function φ_ε in form

$$\varphi_\varepsilon := \frac{1}{1 + \mathrm{e}^{(x-1/2)/\varepsilon}}.$$

In this example the level-set function is not reinitialized, therefore the ε is just a parameter in the equation above. Here, it is not a parameter of the reinitialization.

The discontinuity is imposed at $x = 1/2$. In this special case the jump functional a_2 takes simple form

$$a_{2,\varepsilon}(j_{h,\varepsilon}, \tau) := \int_\Omega g_0 \tau \operatorname{grad} \varphi_\varepsilon \,\mathrm{d}x\,.$$

For the one-dimensional case the finite element space $\mathcal{BDM}_k$ reduces simply to $\mathcal{CG}_k$ element, i.e. Lagrange element of polynomial degree k.

To give a picture how the exact solution and level-set discrete solutions looks like Figures 5.1 and 5.2 are included.

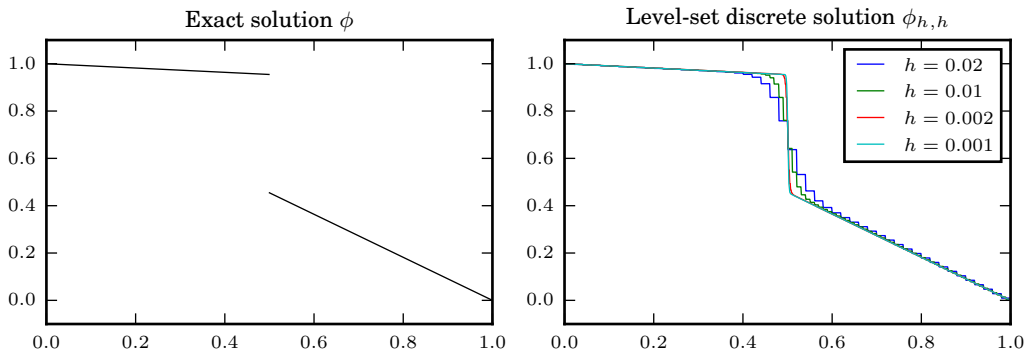

Figure 5.1: Exact and approximate solutions for ϕ.
Approximate solutions $\phi_{h,\varepsilon}$ where the epsilon parameter was set as $\varepsilon = h$, finite element spaces used are $\mathcal{CG}_1 \times \mathcal{DG}_0$ and the jump $g_0 = 1/2$. Several mesh parameters h are plotted in the right figure.

More accurate convergence results are obtained in terms of (absolute error) quantities

$$e_\phi := \|\phi - \phi_{h,\varepsilon}\|_{\mathrm{L}^2}, \quad e_j := \|j - j_{h,\varepsilon}\|_{\mathrm{L}^2}. \tag{5.2}$$

Obtained convergences are plotted in Figure 5.3.

The convergence behaviour for $\phi_{h,\varepsilon}$ and $j_{h,\varepsilon}$ in this simple case is independent of the order k of utilised elements $\mathcal{CG}_k \times \mathcal{DG}_{k-1}$.

For the $j_{h,\varepsilon}$, the order of convergence is found to be approximately 1. For potential $\phi_{h,\varepsilon}$ the order of convergence is found to be 1/2. We present here a simple reasoning for this behaviour.

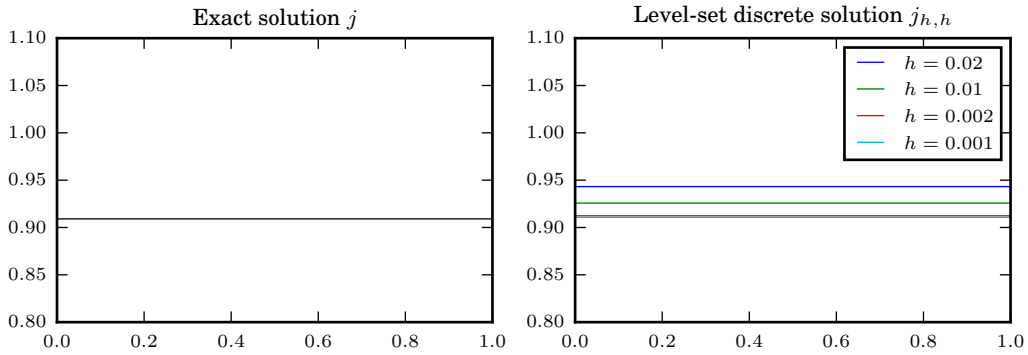

Figure 5.2: Exact and approximate solutions for j.

Approximate solutions $\jmath_{h,\varepsilon}$ where the epsilon parameter was set as $\varepsilon = h$, finite element spaces used are $\mathcal{CG}_1 \times \mathcal{DG}_0$ and the jump $g_0 = 1/2$. Several mesh parameters h are plotted in the right figure.

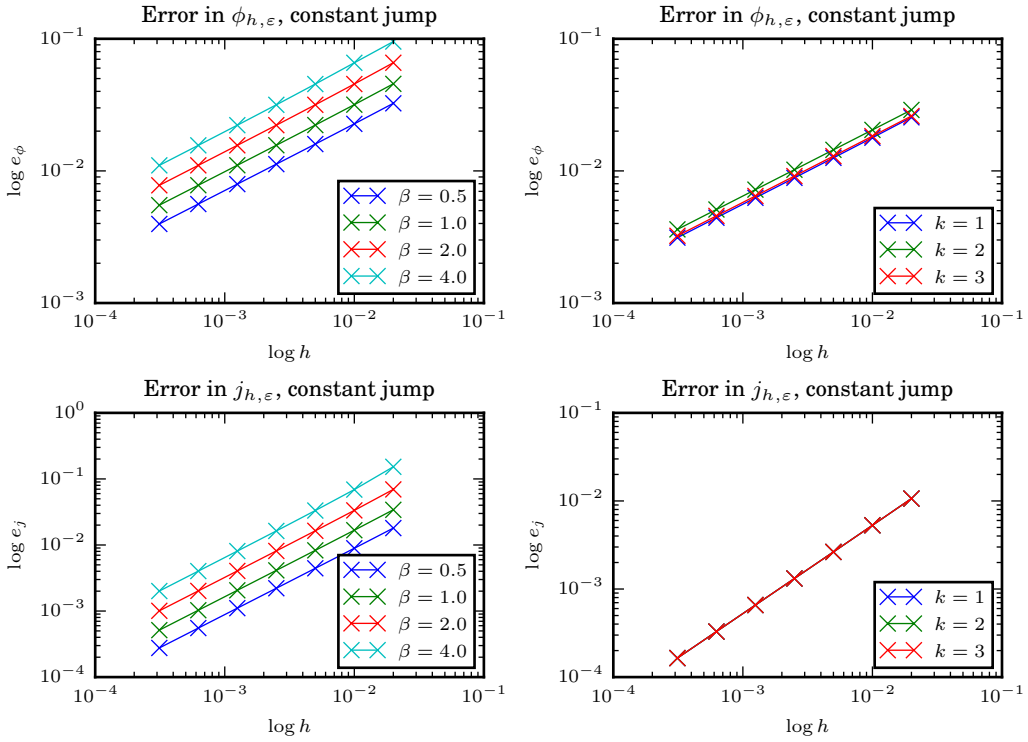

Figure 5.3: Convergence of approximate solutions for one dimensional constant jump with $\varepsilon = \beta h$.

Convergence for various β parameters is shown on left. Several orders k of finite element spaces $\mathcal{CG}_k \times \mathcal{DG}_{k-1}$ are depicted on the right. The order of convergence p of $\phi_{h,\varepsilon}$ is approximately the same for all included cases, e.g. for $\beta = 4, k = 1$ we found $p = 0.519 \pm 0.003$. The order of convergence r for $j_{h,\varepsilon}$ is also approximately the same for all included cases, and e.g. for $\beta = 4, k = 1$ we found $r = 1.03 \pm 0.01$.

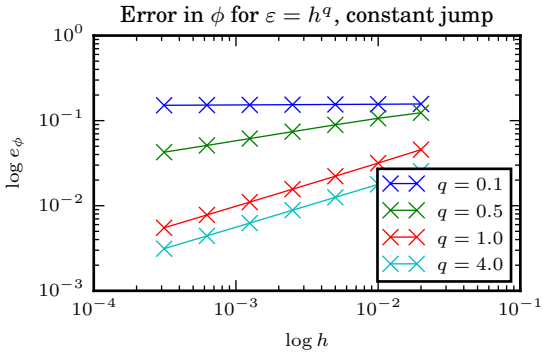

Figure 5.4: Convergence of approximate solutions for one dimensional constant jump with $\varepsilon = h^q$.

Convergence for various q parameters is shown. Finite element spaces used are $\mathcal{CG}_1 \times \mathcal{DG}_0$.

First of all, we have to understand the approximation properties of the level-set as a smooth function. Indeed we can compute

$$\left\|\chi_{(0,1/2)} - \varphi_\varepsilon\right\|_{\mathrm{L}^2}^2 = \int_0^{1/2} \left(1 - \frac{1}{1+\mathrm{e}^{\frac{x-1/2}{\varepsilon}}}\right)^2 \mathrm{d}x + \int_{1/2}^{1} \left(\frac{1}{1+\mathrm{e}^{\frac{x-1/2}{\varepsilon}}}\right)^2 \mathrm{d}x =$$

$$\frac{1}{2} + 2\varepsilon \log 2 + \frac{\varepsilon}{1+\mathrm{e}^{\frac{1}{2\varepsilon}}} + \frac{\varepsilon}{1+\mathrm{e}^{\frac{-1}{2\varepsilon}}} - \varepsilon(\log\left(1+\mathrm{e}^{\frac{-1}{2\varepsilon}}\right) + \log\left(1+\mathrm{e}^{\frac{1}{2\varepsilon}}\right)).$$

For $\varepsilon \longrightarrow 0^+$ the constant term $1/2$ cancels with the term $-\varepsilon \log\left(1+\mathrm{e}^{\frac{1}{2\varepsilon}}\right)$ and all the remaining terms are of leading order $\mathcal{O}(\varepsilon)$. That finally implies $\left\|\chi_{(0,1/2)} - \varphi_\varepsilon\right\|_{\mathrm{L}^2}$ is of order $\mathcal{O}(\varepsilon^{1/2})$.

This means, that if the mesh is refined enough, i.e. there are sufficiently many nodes within the interface region, convergence is of order $1/2$. No discretization effect is present. This is mimicked in Figure 5.3 on left top. Increasing the β parameter one gets more refined mesh but convergence doesn't improve. We are limited with the smooth approximation properties.

If we set $\varepsilon := \beta h^q$ we expect the convergence to improve with increasing q. This is in agreement with Figure 5.4 but only for limited q. For $q > 1$ the convergence doesn't improve and is of order approx. $1/2$. This fits nicely into our picture. For $q < 1$ the level-set thickness is much smaller than mesh element diameter h and the error comes from the interpolation of discontinuity over one element.

According to [Boffi et al., 2013] the convergence for a Poisson equation in mixed setting with $(\mathcal{BDM}_k, \mathcal{DG}_{k-1})$ is of order $\mathcal{O}(h^k)$. On the other hand, our simple 1D example is exactly solvable with piece-wise affine function (in sharp interface limit). It means, that the finite element discretization error is at the level of machine precision ($\approx 10^{-16}$).

We can conclude this study with observation, that no matter what order of spaces k is used the best achievable convergence for $\phi_{h,\varepsilon}$ in this example is of

order 1/2 and for $j_{h,\varepsilon}$ is of order 1. Moreover, this convergence rate limit is due to level-set approximation properties.

5.2 Porous structure growth

5.2.1 Understanding the basic mechanism

We can finally step back to the full electrochemical problem after a "little excursion" to the mathematical and numerical world.

Let us recall the motivation again. When a metal piece (we talked mostly about titan, Ti) is sunk into an electrolyte and external potential difference is applied we can see new oxide layer being formed. Zoomed experimental setup would after some time looks like Figure 2.2. This picture shows a planar geometry and so far only planar geometry was discussed. It is postulated in the paper [Parkhutik and Shershulsky, 1992] (and many other derived papers) that nonplanar geometries could lead to the growth of so called porous or tubular structure during the anodic oxidation.

The basic mechanism for the growth of non-planar geometries is the increase in electric field in the vicinity of the perturbed geometry. Roughly speaking, increased electric field stimulates electrochemical reaction on the interface and total current density $\boldsymbol{j}$ is also increased. Total current density is composed of contributions from metal and oxide ions due to (2.17). Knowing total current density we can add new oxide (or dissolve the oxide) according to (2.18) for the OE interface. Let us study this relation in detail.

We denote here $\boldsymbol{j}^{\mathrm{OE}} \cdot \boldsymbol{n} =: j, \boldsymbol{v}_{\mathrm{OE}} \cdot \boldsymbol{n} =: v$ for brevity. With the use of (2.20) and (2.21) we can write total current density as a function (this function will be denoted $\tilde{j}$) of the surface overpotential

$$j = \tilde{j}(\eta_{s,\mathrm{OE}}) = i_{0,\mathrm{O}^{2-}} \left[\exp\left(\frac{\alpha_{a,\mathrm{O}^{2-}} F}{RT} \eta_{s,\mathrm{OE}} \right) - \exp\left(-\frac{\alpha_{c,\mathrm{O}^{2-}} F}{RT} \eta_{s,\mathrm{OE}} \right) \right] + \\ + i_{0,\mathrm{Ti}^{4+}} \left[\exp\left(\frac{\alpha_{a,\mathrm{Ti}^{4+}} F}{RT} \eta_{s,\mathrm{OE}} \right) \right]. \tag{5.3}$$

With the use of (2.20) and (2.21) we can also write the current efficiency as a function of the surface overpotential,

$$\varepsilon = \tilde{\varepsilon}(\eta_{s,\mathrm{OE}}) = \frac{i_{0,\mathrm{O}^{2-}} \left[\exp\left(\frac{\alpha_{a,\mathrm{O}^{2-}} F}{RT} \eta_{s,\mathrm{OE}} \right) - \exp\left(-\frac{\alpha_{c,\mathrm{O}^{2-}} F}{RT} \eta_{s,\mathrm{OE}} \right) \right]}{\tilde{j}(\eta_{s,\mathrm{OE}})}$$

and inverting the relation $\tilde{j}$ and plugging into $\tilde{\varepsilon}$ we finally get the current efficiency as a function of total current density, j,

$$\varepsilon = \tilde{\varepsilon}(\tilde{j}^{-1}(j)).$$

This simple arithmetic allows us to write the OE evolution speed as a function of the total current density

$$v = v(j) = (t_O - \tilde{\varepsilon}(\tilde{j}^{-1}(j)))j \frac{M_{\mathrm{TiO_2}}}{4\rho_{\mathrm{TiO_2}} F}. \tag{5.4}$$

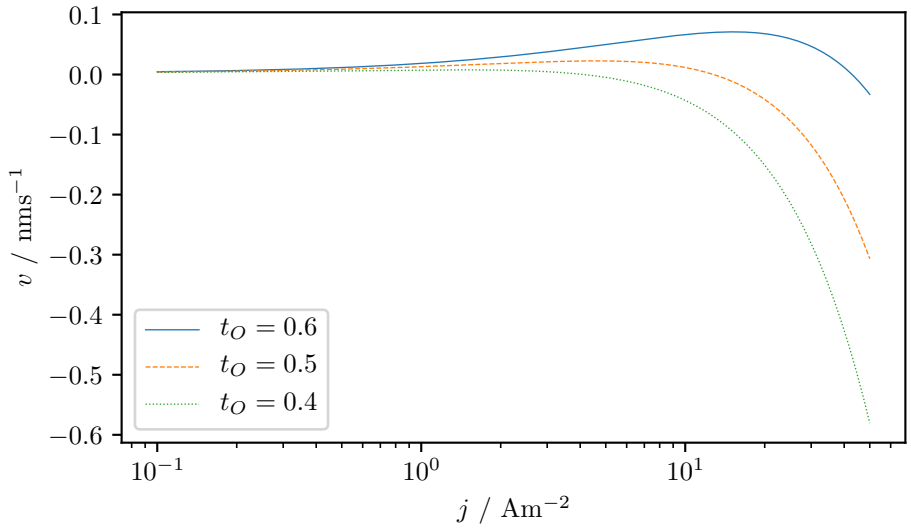

Figure 5.5: Velocity of the OE interface, v, as a function of total current density j.

Several values of oxide transport number t_O are included.

Table 5.1: Constants and parameters used for the basic mechanism illustration.

Constants were taken from [Houser and Hebert, 2006].

M_{TiO_2}	79.866 g mol^{-3}
ρ_{TiO_2}	3.78×10^{6} g m^{-3}
$i_{0,Ti^{4+}}$	20×10^{-2} A m^{-2}
$i_{0,O^{2-}}$	4.9×10^{-2} A m^{-2}
$\alpha_{a,O^{2-}}$	1.9
$\alpha_{c,O^{2-}}$	0.1
$\alpha_{a,Ti^{4+}}$	1.35
F	96485.3329 s A mol^{-1}
R	8.314 J K^{-1} mol^{-1}
T	294 K

In Figure 5.5 the relationship (5.4) is depicted. Constants and parameters used are included in Table 5.1. For low total current densities (< 1 A m^{-2}) the OE interface evolves with negligible speed. Increasing the current density also the velocity increases. Recalling the sign convention, OE interface velocity expresses removal rate, i.e. the oxide layer is dissolved more then formed. The increase is valid up to a point, where removal rate reaches it's maximum. Subsequently,

OE velocity is decreased monotonically. For negative v new oxide layer is formed more then it is dissolved - this results into an overall growth of the oxide phase. There clearly exist a certain value of j for which $v = 0$ and OE is not evolving in time.

This analysis is very important. Whenever there is a little perturbation to the OE interface the electric field is focused in that region. As discussed before - the higher electric field the bigger total current flows. And according to the Figure 5.5 the higher current density the more oxide is removed (up to a point of maximum).

5.2.2 Single perturbation growth

Reinitialization

The first full test case will be the growth of a single perturbation.

Let $\Omega = [0, 1]^2$ be two-dimensional square. In each example we use space $\mathcal{CG}_1$ for high-field potential, $\mathcal{BDM}_1 \times \mathcal{DG}_0$ for mixed formulation of potential and current and space $\mathcal{CG}_1$ for level-set functions.

Let MO and OE interfaces be given by the following level-set functions

$$\varphi_{\mathrm{MO}} = \frac{1}{1 + \exp \frac{x-0.3}{\varepsilon}},$$
$$\varphi_{\mathrm{OE}} = \frac{1}{1 + \exp \frac{x-0.7+0.04\cos(2\pi y)}{\varepsilon}},$$

with $\varepsilon = h$ being minimal mesh cell diameter. In other words, the MO interface is planar and OE interface is perturbed around 0.7 with amplitude 0.04. These function are then interpolated into $\mathcal{CG}_1$ finite element space. According to our solution strategy from Figure 4.5 the following step is reinitialization. Level-set function after reinitialization are included in Figure 5.6.

Zoomed level-set function is depicted in Figure 5.7. Triangularization of the Ω domain is visible. Discretized domain is composed of 100×100 squares divided by both of their diagonals into 4 triangles. This discretization corresponds to $h = 0.001$. In addition, we have plotted $0.1, 0.5$ and 0.9 contours. Recall, that 0.5 contour defines the position of the interface. From this picture we can see, that there are approximately 8 triangles per interfacial layer.

High-field conduction law

We could solve the high-field conduction law in this geometry. For this purpose let us specify physical constants and parameters, see Table 5.2.

The referential length scale is set to $x_{\mathrm{ref}} = 900\,\mathrm{nm}$ which means that our Ω domain is a $900\,\mathrm{nm} \times 900\,\mathrm{nm}$ square. High-field conduction law solution, the potential $\bar{\phi}$, is plotted in Figure 5.8. Expected drop of the potential from $60\,\mathrm{V}$ to $0\,\mathrm{V}$ is evident. This drop occurs solely in the oxide layer, because oxide has the lowest expected conductivity. The conductivity is showed in Figure 5.9. It is also clearly visible, that conductivity is equal to $1 \times 10^{-2}\,\Omega^{-1}\mathrm{m}^{-1}$ in both metal and electrolyte subdomains. Additionally, conductivity in oxide region is approx. 5 orders smaller. Because of several orders difference in conductivity, we have included plot rescaled to the oxide layer, see Figure 5.9 (bottom).

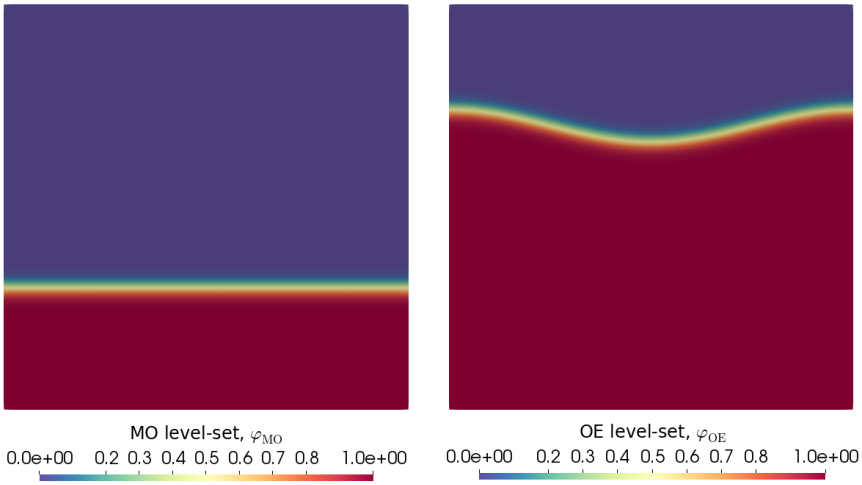

Figure 5.6: Level-set functions after reinitialization.

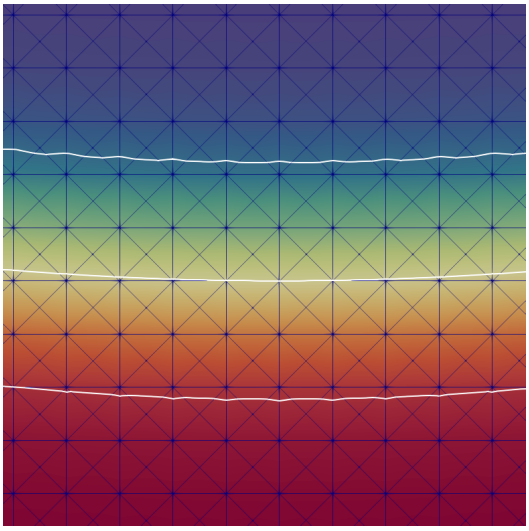

Figure 5.7: Zoomed interfacial region of the level-set function.
Note the triangularization. There are approximately 8 triangles spanning the width of the interface.

This picture shows an increase in conductivity near the perturbation. We could compute total current density due to (2.1). Magnitude of a current computed this way is included in Figure 5.10. This total current density could be then plugged into the (5.4) to obtain the velocity of OE interface (or similarly for the MO interface). This would be, roughly speaking, the approach from [Houser and Hebert, 2006].

However, we do not use this potential for the interfacial evolution. Unlike the paper mentioned, we expect a jump in a solution to play an important role. For that reason a discontinuous potential (mixed formulation) must be solved.

Table 5.2: Constants and parameters used in single pore growth example.
Constants were taken from [Houser and Hebert, 2006].

x_{ref}	900 nm
ϕ_{bottom}	60 V
ϕ_{top}	0 V
σ_m	$1 \times 10^{-2}\ \Omega^{-1}\,\text{m}^{-1}$
σ_e	$1 \times 10^{-2}\ \Omega^{-1}\,\text{m}^{-1}$
$C_{\text{O}^{2-}}$	$9 \times 10^{4}\ \text{mol}\,\text{m}^{-3}$
$C_{\text{Ti}^{4+}}$	$4.5 \times 10^{4}\ \text{mol}\,\text{m}^{-3}$
$u^0_{\text{O}^{2-}}$	$1 \times 10^{-5}\ \text{A}\,\text{m}\,\text{mol}^{-1}$
$u^0_{\text{Ti}^{4+}}$	$1 \times 10^{-5}\ \text{A}\,\text{m}\,\text{mol}^{-1}$
$z_{\text{O}^{2-}}$	2
$z_{\text{Ti}^{4+}}$	4
a	0.1 nm
F	$96485.3329\ \text{s}\,\text{A}\,\text{mol}^{-1}$
R	$8.314\ \text{J}\,\text{K}^{-1}\,\text{mol}^{-1}$
T	294 K

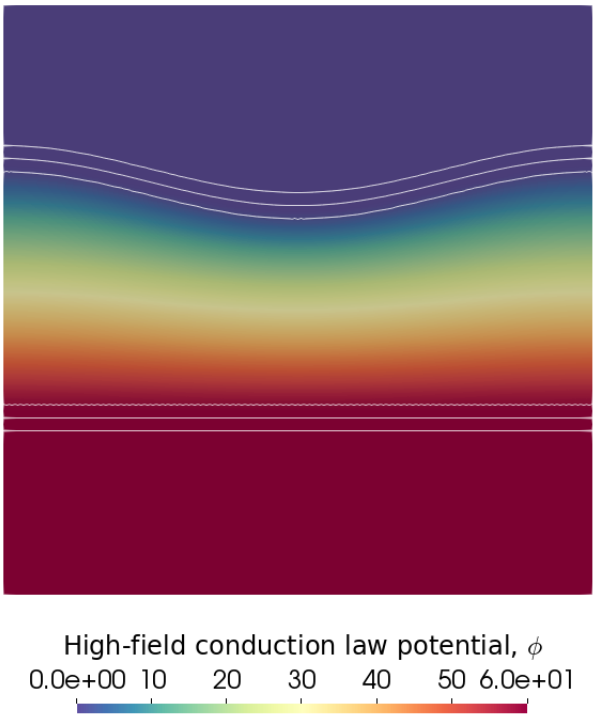

Figure 5.8: High-field conduction law potential in V.
Contours (0.1, 0.5 and 0.9) of level-set functions are included.

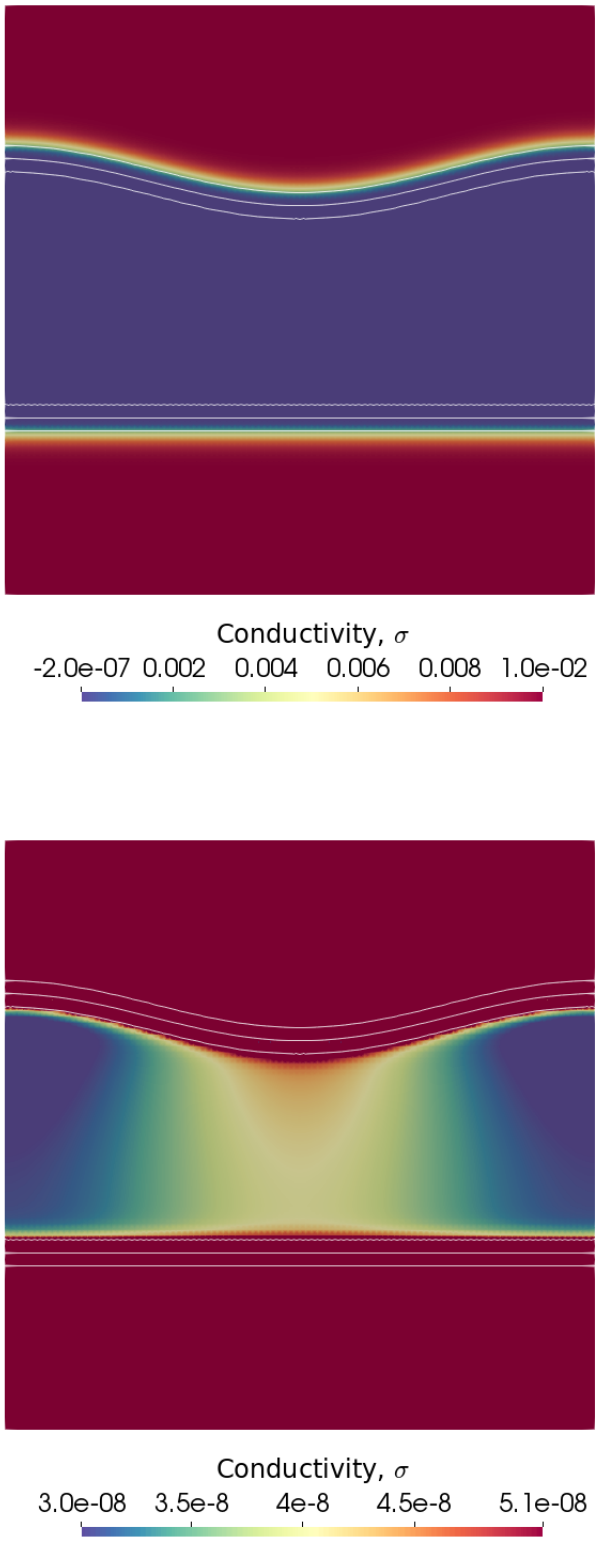

Figure 5.9: High-field conductivity in $\Omega^{-1}\mathrm{m}^{-1}$.
Fully scaled (top) and locally (to the oxide region) rescaled (bottom) plots are included. Contours (0.1, 0.5 and 0.9) of level-set functions are also included.

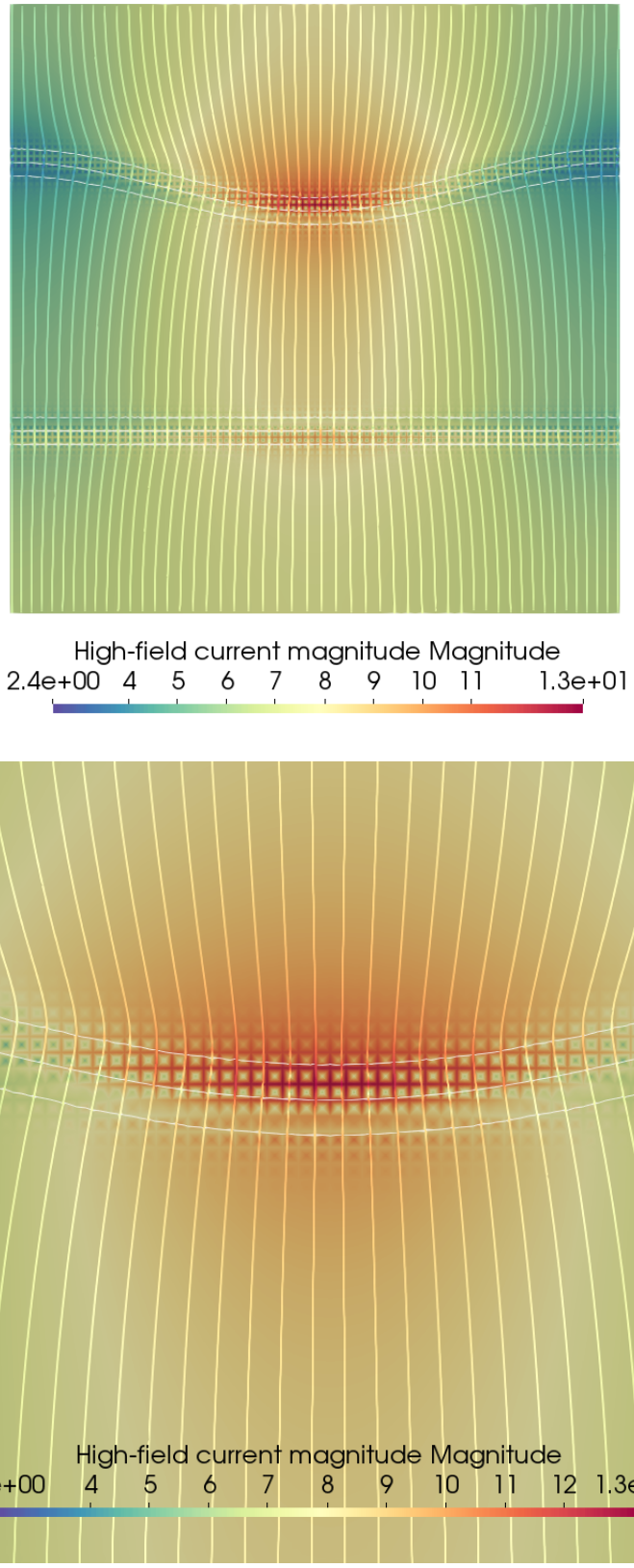

Figure 5.10: High-field current magnitude with streamlines in $\mathrm{A\,m^{-2}}$. Note in the bottom zoomed picture the spurious oscillatory effect in the interfacial region. This is related to the high level-set function gradients in this region. Contours (0.1, 0.5 and 0.9) of level-set functions are also included.

Mixed formulation

The previous computations are used to find a proper conductivity inside oxide domain. We take σ and solve the mixed problem (4.7) and (4.8). In the mixed formulation one must express the jump in potential as a function of the total current density. We denoted this dependence g_{OE} in the previous chapters.

This dependence is nothing but the inverse of relation (5.3). Unfortunately, we are unable to write the inverse function in a closed form. This bring many complications to the numerical computation. We would need to compute the inverse relation numerically. In addition, this inverse relation maps the sought function non-linearly. Because the non-linear problem is solved with the use of Newton-Raphson method one must differentiate this inverse function.

Because of these complications we choose simpler (exactly invertible) version of the Butler-Volmer kinetic relation in form

$$j = \tilde{j}([[\phi]]) = i_{0,\mathrm{O}^{2-}} \sinh\left[\frac{\alpha_{a,\mathrm{O}^{2-}} F}{RT}[[\phi]]\right]$$

with its inverse

$$[[\phi]] = g_{\mathrm{OE}}(j) = \frac{RT}{\alpha_{a,\mathrm{O}^{2-}} F} \log\left[\frac{j}{i_{0,\mathrm{O}^{2-}}} + \sqrt{1 + \left(\frac{j}{i_{0,\mathrm{O}^{2-}}}\right)^2}\right].$$

Solving the mixed problem we get the mixed formulation potential and mixed formulation current. The current is showed in Figure 5.11. Note the difference between (classical) high-field conduction current in Figure 5.10 and this current. Mixed formulation do not cause unwanted oscillatory effects inside interfacial region. Not only this formulation enforces electrochemically valid jump in the potential but the results are more stable from numerical point of view.

Reaction equation and time loop

We have finally the correct total current density in hand from the earlier subsection. Considering the solution strategy, Figure 4.5, the last step is interface evolution.

Although we simplified the Butler-Volmer relation (g_{OE}) in the mixed formulation because of the implementation problems, we do not need to simplify this relation when computing the current efficiency to obtain the OE reaction rate, r_{OE}. This is very important. Even if the jumps are slightly different from the full electrochemical picture, the interface velocity is evaluated correctly and has the desired profile as in Figure 5.5.

Time solution is shown in Figure 5.12. After time 335 s the MO interface approaches bottom boundary and simulation must be terminated.

We changed the geometry (extended the Ω domain to $[0,1] \times [0,2]$ to see the single pore evolution in further time steps. Electrochemical constants are the same as in previous example (Table 5.2) but initial perturbation amplitude is changed to 0.1. Contours of level-set functions are shown in Figure 5.13. In addition, mixed formulation potential is shown in Figure 5.14.

5.2.3 Multiple pores growth

In the last section we will present evolution of perturbations from different initial geometries.

Our domain Ω is again $[0,1]\times[0,2]$ rectangle. The initial level-set functions are chosen in a similar way to the previous experiments. The MO interface is initially planar and OE interface is sinusoidally perturbed. Electrochemical constants are (if not specified otherwise) the same as in Table 5.2.

First example is the growth of two initial perturbations. Results are depicted in Figures 5.15, 5.16. We can see how two perturbations start to grow. Before the MO interface reaches the bottom computational boundary perturbations become unstable and start to split ($t = 4000\,\mathrm{s}$).

Nice illustration of high-field current is given in Figure 5.17. Note, how the current density is increased at the bottom of the perturbations. The higher current density the more is oxide dissolved (up to a maximum point) - due to the basic mechanism.

We can add another initial perturbation to the geometry. Again, results are shown in Figures 5.18, 5.19, 5.20. In the final computational time the pores are beginning to split.

We introduced the transport number t_O in the electrochemical section. The previous results are all computed with transport number set to 0.6. From the basic mechanism illustration, see Figure 5.5, if we set the transport number to $t_O = 0.4$ we expect the OE velocity be always negative (only addition of new oxide layer due to the sign convention). Indeed, this is demonstrated in Figure 5.21. You can see how initially perturbed OE interface gets straightened. In addition, the perturbations are not growing and the only evolving interface is the MO. After some time even the speed of MO interface halts. This is due to the fact, that growing oxide layer decreases total current density.

Recall, that the level-set thickness is given by the minimal mesh cell diameter h. This means, that if we refine the mesh to $h = 0.0067$ the level-set transition region shrinks. The effect of mesh density on our results is shown in Figure 5.22. For the times $t < 1500\,\mathrm{s}$ no significant change is visible. Results are mesh independent. However, when the bottom of the pore get more and more flattened it begins to split and this splitting seems to be dependent on the discretization parameters.

The reason for the fact, that the perturbations doesn't maintain their profile and gets dissected is clear from Figure 5.5. Consider the solid (blue) line with $t_O = 0.6$. Until a point of maximum the OE velocity vs. current density function is increasing. This means, that the higher current density the more is oxide removed. Sinusoidal perturbation has the highest current density near its bottom tip, so the higher the interfacial curvature, the faster is the tip moving. However, when current density exceeds the maximum point of the solid (blue) line, the OE velocity vs. current density function in decreasing. And this has substantial effects. Sharp tip of a perturbation is moving more slowly than less curved vicinity of the tip. It results in the flattening of the pore bottom and consecutive splitting.

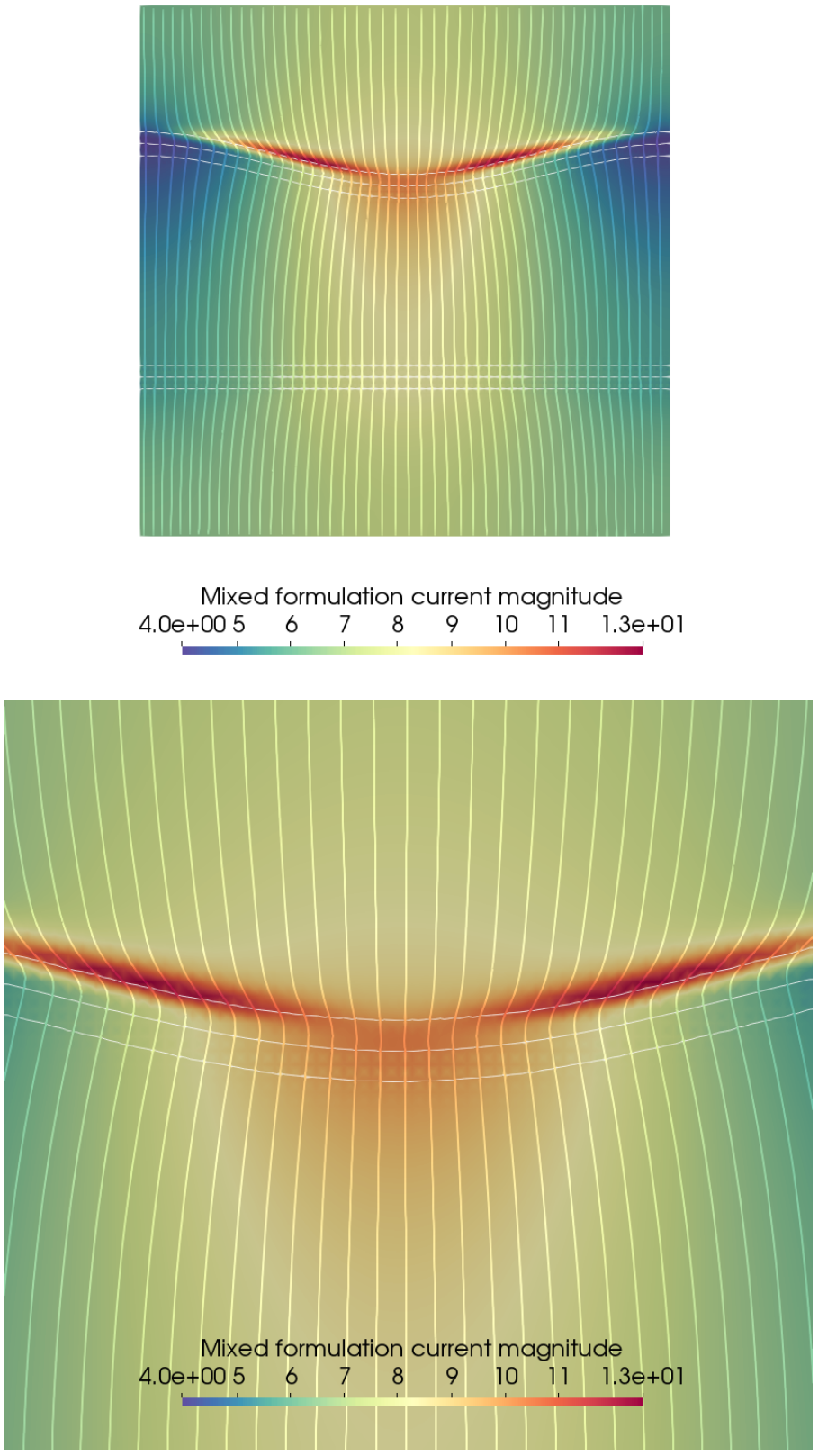

Figure 5.11: Mixed formulation current magnitude with streamlines in $\mathrm{A\,m^{-2}}$. Note in the bottom zoomed picture without the spurious oscillatory effect in the interfacial region. Contours (0.1, 0.5 and 0.9) of level-set functions are also included.

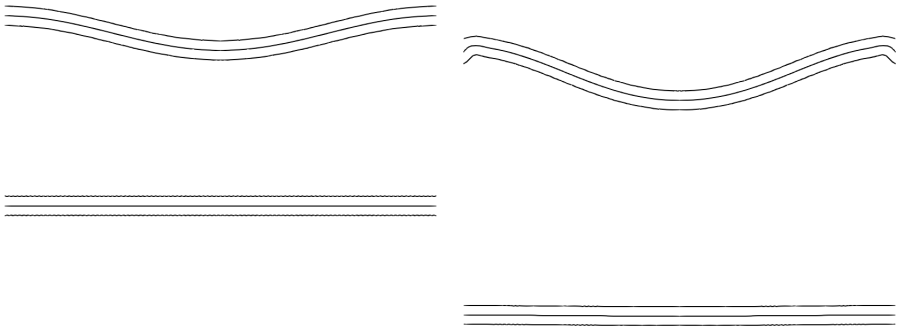

Figure 5.12: Evolution of OE and MO interfaces for single pore experiment.
Initial configuration is shown on the left ($t = 0\,\mathrm{s}$). On the right interfaces after 335 s are portrayed. Contours (0.1, 0.5 and 0.9) of level-set functions are included.

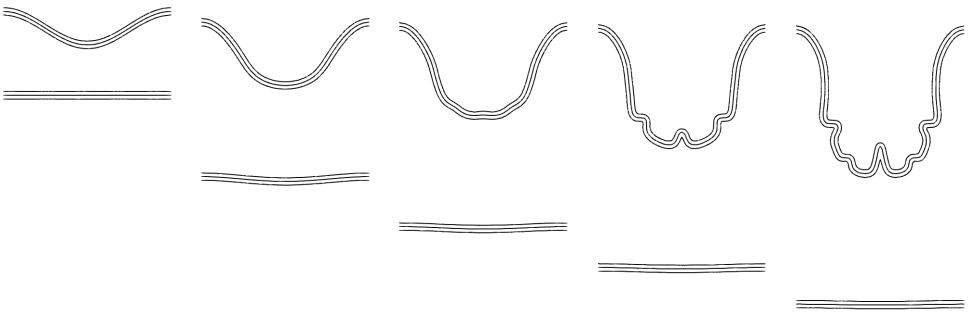

Figure 5.13: Evolution of OE and MO interfaces for single pore experiment with extended geometry.
Contours at times (from left to right) $t = 0\,\mathrm{s}, 1000\,\mathrm{s}, 2000\,\mathrm{s}, 3000\,\mathrm{s}, 4000\,\mathrm{s}$. Contours (0.1, 0.5 and 0.9) of level-set functions are included.

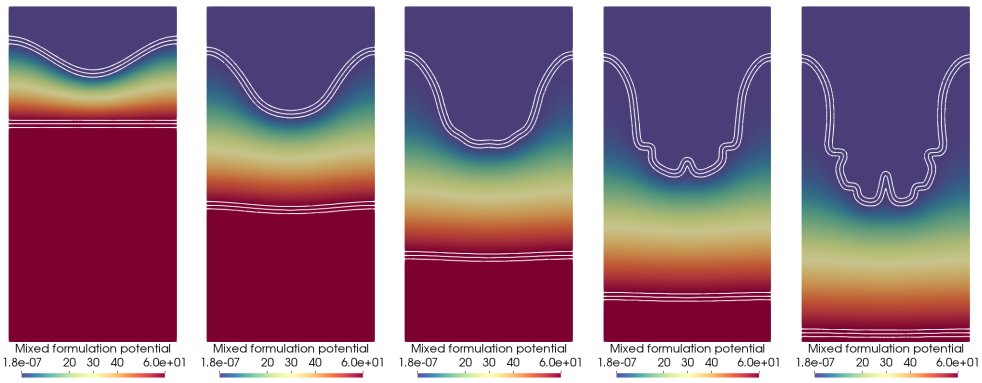

Figure 5.14: Mixed formulation potential for single pore experiment with extended geometry in V.

Potential at times (from left to right) $t = 0\,\text{s}, 1000\,\text{s}, 2000\,\text{s}, 3000\,\text{s}, 4000\,\text{s}$. Contours (0.1, 0.5 and 0.9) of level-set functions are also included.

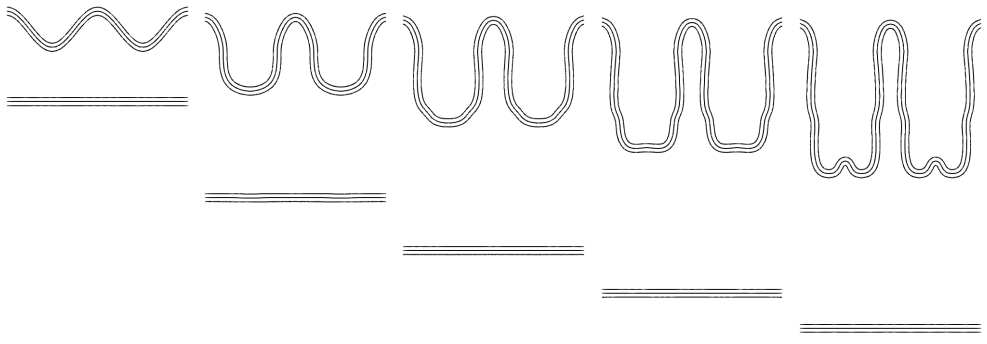

Figure 5.15: Evolution of OE and MO interfaces for two perturbations experiment.

Contours at times (from left to right) $t = 0\,\text{s}, 1000\,\text{s}, 2000\,\text{s}, 3000\,\text{s}, 4000\,\text{s}$. Contours (0.1, 0.5 and 0.9) of level-set functions are included.

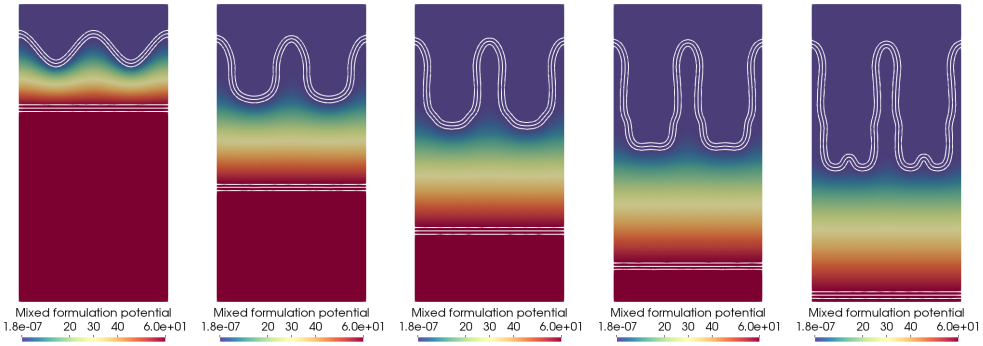

Figure 5.16: Mixed formulation potential for two perturbations experiment in V.

Potential at times (from left to right) $t = 0\,\mathrm{s}, 1000\,\mathrm{s}, 2000\,\mathrm{s}, 3000\,\mathrm{s}, 4000\,\mathrm{s}$. Contours (0.1, 0.5 and 0.9) of level-set functions are also included.

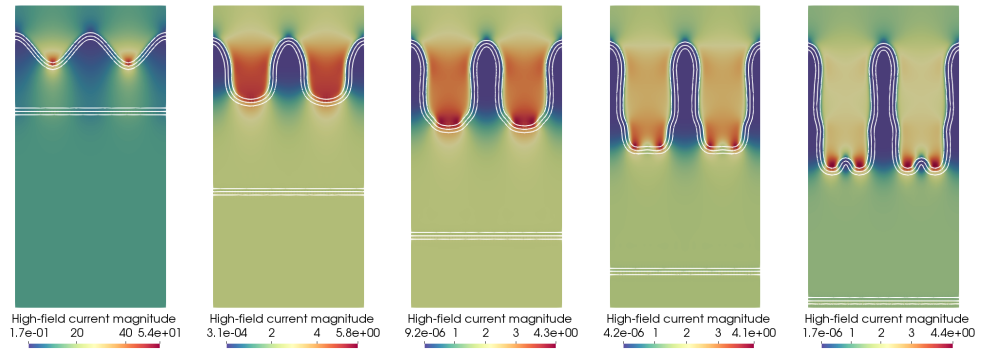

Figure 5.17: High-field current for two perturbations experiment in $\mathrm{A\,m^{-2}}$.

Current at times (from left to right) $t = 0\,\mathrm{s}, 1000\,\mathrm{s}, 2000\,\mathrm{s}, 3000\,\mathrm{s}, 4000\,\mathrm{s}$. Contours (0.1, 0.5 and 0.9) of level-set functions are also included.

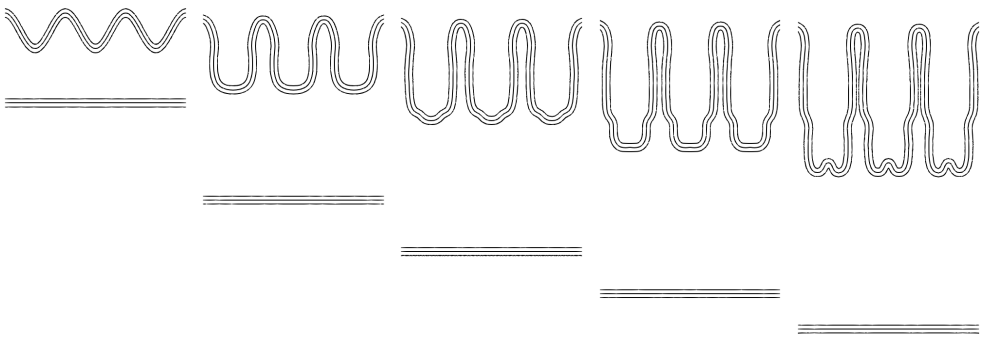

Figure 5.18: Evolution of OE and MO interfaces for three perturbations experiment.

Contours at times (from left to right) $t = 0\,\text{s}, 1000\,\text{s}, 2000\,\text{s}, 3000\,\text{s}, 4000\,\text{s}$. Contours (0.1, 0.5 and 0.9) of level-set functions are included.

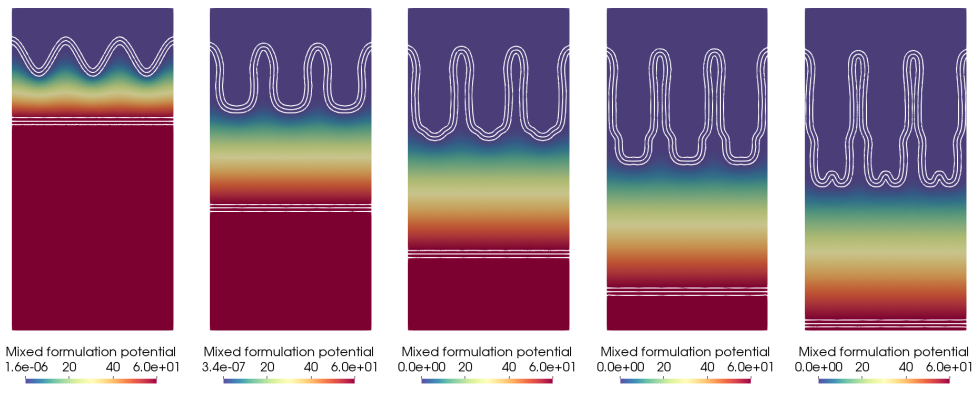

Figure 5.19: Mixed formulation potential for three perturbations experiment in V.

Potential at times (from left to right) $t = 0\,\text{s}, 1000\,\text{s}, 2000\,\text{s}, 3000\,\text{s}, 4000\,\text{s}$. Contours (0.1, 0.5 and 0.9) of level-set functions are also included.

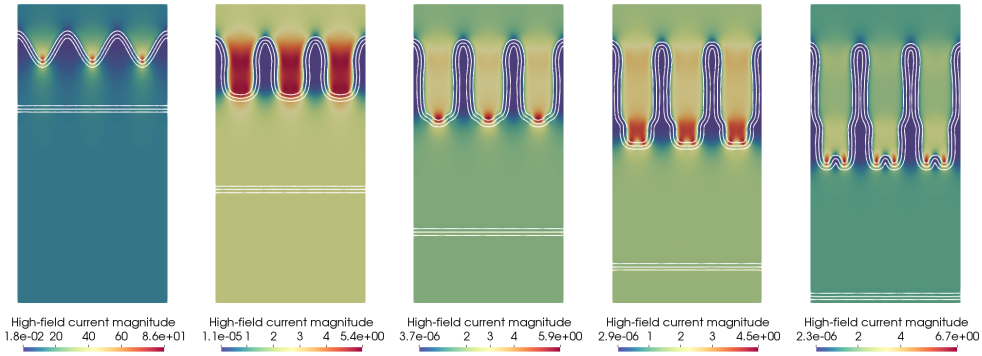

Figure 5.20: High-field current for three perturbations experiment in $\mathrm{A\,m^{-2}}$.
Current at times (from left to right) $t = 0\,\mathrm{s}, 1000\,\mathrm{s}, 2000\,\mathrm{s}, 3000\,\mathrm{s}, 4000\,\mathrm{s}$. Contours (0.1, 0.5 and 0.9) of level-set functions are also included.

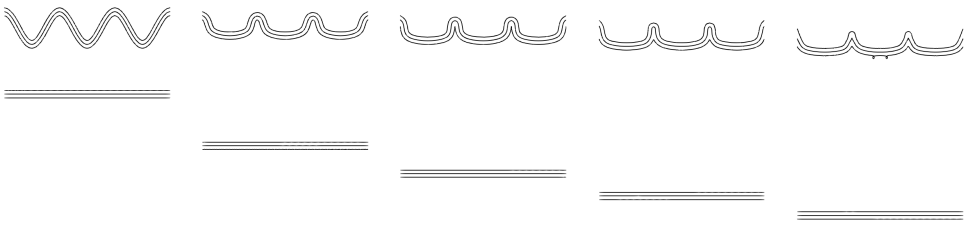

Figure 5.21: Evolution of OE and MO interfaces for three perturbations experiment. Oxide transport number is set to $t_O = 0.4$.
Contours at times (from left to right) $t = 0\,\mathrm{s}, 1000\,\mathrm{s}, 2000\,\mathrm{s}, 3000\,\mathrm{s}, 4000\,\mathrm{s}$. Contours (0.1, 0.5 and 0.9) of level-set functions are included.

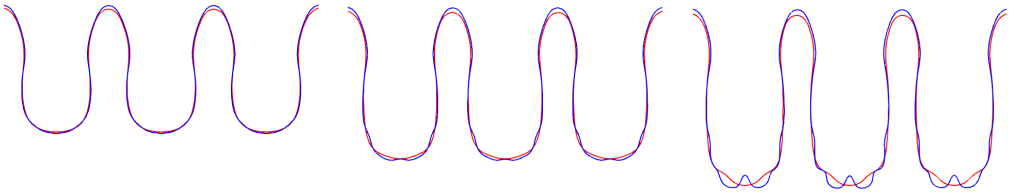

Figure 5.22: Illustration of level-set thickness dependence.
Contour (0.5) of level-set functions is shown. Red line corresponds to discretization parameter $h = 0.01$, blue line to a finer mesh with $h = 0.0067$. Times $t = 1000\,\mathrm{s}, 1500\,\mathrm{s}, 2000\,\mathrm{s}$ are included.

Appendices

A. Appendix

Theorem 1 (Normal traces of $\mathrm{H}(\mathrm{div}, \Omega)$)**.** *Let Ω be a bounded domain in $\mathbb{R}^d$ with Lipschitz-continuous boundary Γ. Then there exists a linear, bounded and surjective operator $\mathrm{Tr}_{\boldsymbol{n}_\Gamma} : \mathrm{H}(\mathrm{div}, \Omega) \longrightarrow \mathrm{H}^{-1/2}(\Gamma)$ such that for each $\boldsymbol{\tau} \in [\mathrm{H}^1(\Omega)]^d$ the $\mathrm{Tr}_{\boldsymbol{n}_\Gamma}(\boldsymbol{\tau})$ is identified through the inner product of $\mathrm{L}^2(\Gamma)$ with $\mathrm{Tr}\, \boldsymbol{\tau} \cdot \boldsymbol{n}_\Gamma$.*

Proof. See [Gatica, 2014], Theorem 1.7. □

Theorem 2 (Green's identity in $\mathrm{H}(\mathrm{div}, \Omega)$)**.** *Let Ω be a bounded domain in $\mathbb{R}^d$ with Lipschitz-continuous boundary Γ. Then there holds*

$$\langle \mathrm{Tr}_{\boldsymbol{n}_\Gamma}(\boldsymbol{\tau}), \mathrm{Tr}\, w \rangle_{\mathrm{H}^{-1/2}, \mathrm{H}^{1/2}} = \int_\Omega \boldsymbol{\tau} \cdot \mathrm{grad}\, w \, \mathrm{d}x + \int_\Omega w \, \mathrm{div}\, \boldsymbol{\tau} \, \mathrm{d}x \,, \qquad \forall w \in \mathrm{H}^1(\Omega), \quad \boldsymbol{\tau} \in \mathrm{H}(\mathrm{div}, \Omega).$$

Proof. See [Gatica, 2014], Lemma 1.4. □

Theorem 3 (Non-linear Lax-Milgram lemma)**.** *Let V be a Hilbert space, $A : V \longrightarrow V^*$ be strongly monotone and Lipschitz continuous. Then for all $f \in V^*$ there exists a unique solution $u \in V$ such that*

$$A(u) = f.$$

Proof. Simple exercise on the use of the Banach fixed-point theorem. See [Roubíček, 2013], Proposition 2.22. □

Definition 1 (Strongly monotone mapping)**.** *Let V be a Banach space and let $A : V \longrightarrow V^*$. We call A strongly monotone iff*

$$\langle A(u) - A(v), u - v \rangle_{V^*, V} \geq \|u - v\|_V^2$$

for all $u, v \in V$.

Definition 2 (Lipschitz continuous mapping)**.** *Let V be a Banach space and let $A : V \longrightarrow V^*$. We call A Lipschitz continuous iff there exists $L > 0$ such that*

$$\|A(u) - A(v)\|_{V^*} \leq L \|u - v\|_V$$

for all $u, v \in V$.

Conclusion

This thesis is a compilation of results from different parts of physics, chemistry and mathematics.

The work is composed of 5 chapters. In the first chapter a history and current state of research are outlined. Few applications are mentioned there also.

The second chapter deals with detailed electrochemical picture. It is written without any assumption on previous electrochemistry knowledge. Reaction pathways occurring in the half-cell experiment are thoroughly discussed. Basic terms such as overpotential, potential, electrochemical potential, etc. are introduced. Additionally, Butler-Volmer relations are explained and the whole picture is summarized into the overall solution procedure.

The aim of the third chapter is to formulate equations from the second chapter in a mathematically more precise, rigorous way. In this stage only infinite-dimensional abstract problems are formulated. In addition, we derive a mixed formulation for a solution to the Laplace equation with a jump inside the solution domain. Existence and uniqueness of the solution to this problem is proved.

Fourth chapter intents to discretize the infinite-dimensional equations in a numerically stable way. A method for interface tracking, the characteristic level-set method, is introduced. With the help of this method interfacial integrals are approximated.

Last chapter demonstrates the performance of overall model. It starts with step-by-step solution to a single pore growth example. Later, multiple pores and more complex geometries are simulated.

In summary, the problem of metal oxide growth is very complex. None of the overall solution steps could be neglected and this makes the problem very difficult to solve. There are several simplifications in our model. Let us list disadvantages of this model:

- High-field conduction potential is sought continuous. In a proper simulation one would merge high-field computation with mixed formulation. Unfortunately, our mixed formulation doesn't allow both.

- Reaction pathways are debatable. There are many papers each having different point of view on the electrochemical nature of the process. In addition, parameters and constant do not always have clear physical meaning, nor are measurable.

- Characteristic level-set method is in some cases sensitive to the choice of thickness of the interface. Although our one-dimensional experiments shows nice convergence properties it might not be the case in general two-dimensional (or three-dimensional) situation.

- Mathematical assumptions on Butler-Volmer relations are not fully resolved. We have to assume, that mapping $g_{\mathrm{MO/OE}}$ improve the normal trace of current density and map it to space $\mathrm{H}^{1/2}$. Similarly, the current efficiency is a non-linear function of the current density's normal component, which doesn't make sense for distributions ($\mathrm{H}^{-1/2}$). Situation is better in finite

dimensional case, because current density has additional smoothness. However, the infinite dimensional abstract case remains open problem.

On the other hand, our general multiphase picture introduces new techniques into the electrochemical world and allows more complex simulation. The advantages and novelties of this model are

- Compact and consistent description of reactions. We present the reaction schema and reaction pathways clearly explained. This is a rare contribution in the field of nanopores modelling.
- Mixed formulation for discontinuous potential. The use of mixed formulation for discontinuous potential in Butler-Volmer driven problems is a novelty. In addition, mathematical side of the problem is also treated.
- Implicit geometry description. The characteristic level-set method allows complex geometrical structures to be grown.

Developed model could be used for simulations under various conditions. However, there is a need to validate the model against experimental data.

Possible future extensions include: validation against experiments, coupling of mixed formulation with high-field conduction law, comparison with other reaction schema.

Bibliography

Martin Alnæs, Jan Blechta, Johan Hake, August Johansson, Benjamin Kehlet, Anders Logg, Chris Richardson, Johannes Ring, Marie E Rognes, and Garth N Wells. The fenics project version 1.5. *Archive of Numerical Software*, 3(100): 9–23, 2015.

Daniele Boffi, Franco Brezzi, and Michel Fortin. *Mixed finite element methods and applications*, volume 44. Springer Science & Business Media, 2013.

Susanne Brenner and Ridgway Scott. *The mathematical theory of finite element methods*, volume 15. Springer Science & Business Media, 2007.

NFMN Cabrera and NF Mott. Theory of the oxidation of metals. *Reports on progress in physics*, 12(1):163, 1949.

Chuan Cheng. *Electro-chemo-mechanics of anodic porous alumina nano-honeycombs: self-ordered growth and actuation*. Springer, 2015.

S DeWitt and K Thornton. Simulations of anodic nanopore growth using the smoothed boundary and level set methods. *The Journal of Physical Chemistry C*, 120(4):2419–2431, 2016.

Stephen DeWitt and Katsuyo Thornton. Model for anodic film growth on aluminum with coupled bulk transport and interfacial reactions. *Langmuir*, 30 (18):5314–5325, 2014.

AT Fromhold Jr. Theory of metal oxidation. vol. i. fundamentals. *North Holland Publishing Co., Amsterdam, New York and Oxford. 1976, 547 p*, 1976.

Gabriel N Gatica. *A simple introduction to the mixed finite element method: theory and applications*. Springer Science & Business Media, 2014.

Andrei Ghicov and Patrik Schmuki. Self-ordering electrochemistry: a review on growth and functionality of tio 2 nanotubes and other self-aligned mo x structures. *Chemical Communications*, (20):2791–2808, 2009.

Craig A Grimes and Gopal K Mor. *TiO2 nanotube arrays: synthesis, properties, and applications*. Springer Science & Business Media, 2009.

Kurt R Hebert and Jerrod E Houser. A model for coupled electrical migration and stress-driven transport in anodic oxide films. *Journal of The Electrochemical Society*, 156(8):C275–C281, 2009.

Kurt R Hebert, Sergiu P Albu, Indhumati Paramasivam, and Patrik Schmuki. Morphological instability leading to formation of porous anodic oxide films. *Nature materials*, 11(2):162–166, 2012.

Jerrod E Houser and Kurt R Hebert. Modeling the potential distribution in porous anodic alumina films during steady-state growth. *Journal of the Electrochemical Society*, 153(12):B566–B573, 2006.

Jerrod E Houser and Kurt R Hebert. The role of viscous flow of oxide in the growth of self-ordered porous anodic alumina films. *Nature materials*, 8(5): 415–420, 2009.

F Keller, MS Hunter, and DL Robinson. Structural features of oxide coatings on aluminum. *Journal of the Electrochemical Society*, 100(9):411–419, 1953.

AG Limonov. Numeric simulation of the formation of hexagonal nanoscale structure arrays in anodic aluminum oxide. *Mathematical Models and Computer Simulations*, 3(2):149–157, 2011.

JM Macak, H Tsuchiya, A Ghicov, K Yasuda, R Hahn, S Bauer, and P Schmuki. Tio 2 nanotubes: self-organized electrochemical formation, properties and applications. *Current Opinion in Solid State and Materials Science*, 11(1):3–18, 2007.

John Newman and Karen E Thomas-Alyea. *Electrochemical systems*. John Wiley & Sons, 2012.

Elin Olsson and Gunilla Kreiss. A conservative level set method for two phase flow. *Journal of computational physics*, 210(1):225–246, 2005.

Elin Olsson, Gunilla Kreiss, and Sara Zahedi. A conservative level set method for two phase flow ii. *Journal of Computational Physics*, 225(1):785–807, 2007.

JP O'sullivan and GC Wood. The morphology and mechanism of formation of porous anodic films on aluminium. In *Proceedings of the Royal Society of London A: Mathematical, Physical and Engineering Sciences*, volume 317, pages 511–543. The Royal Society, 1970.

VP Parkhutik and VI Shershulsky. Theoretical modelling of porous oxide growth on aluminium. *Journal of Physics D: Applied Physics*, 25(8):1258, 1992.

Maggie Paulose, Karthik Shankar, Sorachon Yoriya, Haripriya E Prakasam, Oomman K Varghese, Gopal K Mor, Thomas J LaTempa, Adriana Fitzgerald, and Craig Grimes. Anodic growth of highly ordered tio2 nanotube arrays to 134 μm in length. *The Journal of Physical Chemistry B*, 112(47):15261–15261, 2008.

Tomáš Roubíček. *Nonlinear partial differential equations with applications*, volume 153. Springer Science & Business Media, 2013.

Walter Rudin. *Real and complex analysis*. Tata McGraw-Hill Education, 1987.

C Sample and AA Golovin. Formation of porous metal oxides in the anodization process. *Physical Review E*, 74(4):041606, 2006.

ENDRE Süli. A brief excursion into the mathematical theory of mixed finite element methods. *Lecture Notes, University of Oxford*, pages 24–29, 2013.

KJ Vetter and F Gorn. Kinetics of layer formation and corrosion processes of passive iron in acid solutions. *Electrochimica Acta*, 18(4):321–326, 1973.

List of Figures

List of Tables

List of Abbreviations

MO ..... interface between metal and oxide layer

OE ..... interface between oxide and electrolyte layer